

Chapter 1

Nature of the Spin Glass Phase in Finite Dimensional (Ising) Spin Glasses

Juan J. Ruiz-Lorenzo*

Departamento de Física,

Universidad de Extremadura, 06006 Badajoz, Spain

Instituto de Computación Científica Avanzada de Extremadura (ICCAEx),

Universidad de Extremadura, 06006 Badajoz, Spain

Instituto de Biocomputación y Física de los Sistemas Complejos (BIFI),

50018 Zaragoza, Spain

Spin glasses are the paradigm of complex systems. These materials present really slow dynamics. However, the nature of the spin glass phase in finite dimensional systems is still controversial. Different theories describing the low temperature phase have been proposed: droplet, replica symmetry breaking and chaotic pairs. We present analytical studies of critical properties of spin glasses, in particular, critical exponents at and below the phase transition, existence of a phase transition in a magnetic field, computation of the lower critical dimension (in presence/absence of a magnetic field). We also introduce some rigorous results based on the concept of metastate. Finally, we report some numerical results regarding the construction of the Aizenman-Wehr metastate, scaling of the correlation functions in the spin glass phase and existence of a phase transition in a field, confronting these results with the predictions of different theories.

Contents

1. Introduction	2
2. A brief tour of spin glasses	3
3. Some theoretical results	9
3.1. Mean-field solution	9
3.2. Spin glasses in finite dimensions	15
3.3. The droplet model	15

*ruiz@unex.es

3.4.	Field theory ($h = 0$)	16
3.5.	Field theory ($h \neq 0$)	18
3.6.	Metastate	19
4.	Some numerical results	22
4.1.	Phase transition at $h = 0$	22
4.2.	Behavior of the correlation functions in the spin glass phase	25
4.3.	Metastate: Numerical results	29
4.4.	Phase transition at $h \neq 0$	31
5.	Conclusions	36
A.1.	Characterization of a phase transition: Quotient and fixed coupling methods	38
A.2.	The Janus supercomputers	39
	References	40

1. Introduction

Spin glasses are often considered as the paradigm of complex systems. They show frustration and randomness which are now ubiquitous characteristics in nature. In addition, the role played by spin glasses in magnetism is huge: spin glass behavior jointly with ferromagnetism and antiferromagnetism are the three most frequent forms of “magnetic order”. On the theoretical side, radical approaches to describe them have been developed and in some cases are still needed. Finally, there is great interplay among spin glasses and other systems, from the molecular evolution to astrophysics.¹

This chapter is devoted to the study of properties of spin glasses in finite dimensions (mainly in three dimensions) using analytical and numerical approaches. The main goal is to determine existence of a spin glass phase in finite dimensions and, if it exists, to characterize its physical properties.

We start by describing some basic properties of spin glasses in Sec. 2. Next, this book chapter continues in two main parts.

In the first one, we report the main theoretical results (Sec. 3), starting with the mean-field solution in Sec. 3.1, which already provides a complex picture even in infinite dimensions. Sec. 3.2 is devoted to study to what extent this complex picture survives in finite dimensions. In Sec. 3.3 we report the droplet theory, a phenomenological theory that can also be formulated in terms of the Migdal-Kadanoff approximation of the renormalization group. Hereafter, we resort to the “standard” approach based on a field theory approach built on the complex mean-field solution, describing its main findings both in absence (Sec. 3.4) and in presence of a magnetic field (Sec. 3.5). We finish this part by introducing in Sec. 3.6 an important concept and tool of the metastate.

In the second part of the chapter, we describe numerical simulations at equilibrium (Sec 4). We start to report some important numerical facts in

absence of a magnetic field. First, we show in Sec. 4.1 the existence of a phase transition in three dimensions and how its universality class has been characterized. Once we know there is a spin glass phase in three dimensions, in Sec. 4.2 we present numerical simulations that try to characterize the properties of this phase, in particular, we focus on the behavior of the conditional correlation functions. Next, we continue by showing a numerical construction of the metastate and properties of the spin glass phase one can draw from this powerful tool (Sec. 4.3). We close this part with the study of spin glasses in a field. We focus on the simulations performed in four dimensions and the rationale of the new numerical approaches that have been useful to find the phase transition. However, the phase transition in three dimensions in a field has been elusive even using these new numerical tools (Sec. 4.4).

The book chapter finishes with the conclusions and two appendices. In the first one we report the finite size scaling tools needed to analyze the critical behavior of these systems, namely the quotient method and the analysis at fixed coupling (Sec. A.1). Part of the numerical simulations presented in this chapter have been obtained with the help of Janus I and II supercomputers. In the last appendix, we have described the basic characteristics of these two dedicated computers (Sec. A.2).

This book chapter is based on the lectures given by the author in Lviv during the Ising Lectures 2019 and we have tried to report the contents lectured there during two days. In these two lectures, the focus was on equilibrium numerical simulations on finite dimensional Ising spin glasses. Hence, we have not discussed in this chapter important topics in spin glass physics as experiments and out-of-equilibrium simulations.

Finally, let us mention that it is also possible to study the properties of the low temperature phase with $h = 0$ and $h \neq 0$ by simulating $D = 1$ dimensional Ising spin glass with the coupling decaying following a power law and it has been used for the study of the spin glass phase inside and outside the mean-field region.²⁻¹⁴

2. A brief tour of spin glasses

In this section we describe the main physical properties of these materials.

The main ingredients to obtain materials with a spin glass behavior are magnetic interaction, randomness, frustration and anisotropy.¹ However, materials with spin glass behavior can be obtained in different ways, for example magnetic interaction is not needed.^{1,15-18}

Metals with very diluted magnetic impurities are considered canonical spin glasses. We can mention, for example, CuMn and Ag:Mn at 2.5%, CdCr_{1.7}IN_{0.3}S₄ and Fe_{0.5}Mn_{0.5}TiO₃. In these materials one can identify magnetic interaction and randomness, via the dilution of the magnetic moments.

Since the characteristic times associated with the magnetic impurities are much bigger than the times associated with the electrons of the metal, we can assume that the impurities are *quenched*. This approximation is similar to that performed in molecular physics called Born-Oppenheimer approximation (in molecules the nuclei play the role of the magnetic impurities in spin glasses). It is possible to define another kind of disorder, the so-called *annealed* one, in which the components in the material (“normal” and “impurities”) have similar characteristic times and, thus, the statistical mechanics considers all of them in the same way.

In spin glasses, the magnetic impurities do not interact following the standard exchange interaction, rather, they interact among them via the electrons moving in the conduction band of the metal, the so-called RKKY interaction following the work of Ruderman, Kittel, Kasuya and Yosida.^{19–21} It has been shown that the strength of the interaction, $J(r)$, between two magnetic moments (impurities) sited at distance r is given by^{1,15}

$$J(r) \sim \frac{\cos(2k_F r)}{r^3}, \quad (1)$$

k_F being the Fermi momentum. In addition to a power law decay on the distance of the interaction, an oscillatory factor (the cosine) appears: depending on distance, sometimes it will induce a positive interaction and other times a negative one (see Fig. 1).

This change of the sign of the interaction produces the frustration in the system. In Fig. 2 we show a frustrated square. In this square the product of the four couplings (J_{ij} living in the links) is negative, and thus, there are different spin configurations which provide the same energy: frustration.

The joint effect of disorder and frustration usually produces a very complicated landscape of free energy, and in particular, a very slow dynamics. The landscape depicted in Fig. 3 is typical of glassy systems, showing a great number of relative maxima and minima separated by high free energy barriers.

The last ingredient to build the Ising spin glass model is the anisotropy.¹ For instance Ag:Mn and CdCr_{1.7}IN_{0.3}S₄ are well described by Heisenberg spins, although the description of Fe_{0.5}Mn_{0.5}TiO₃ is based on Ising spins.

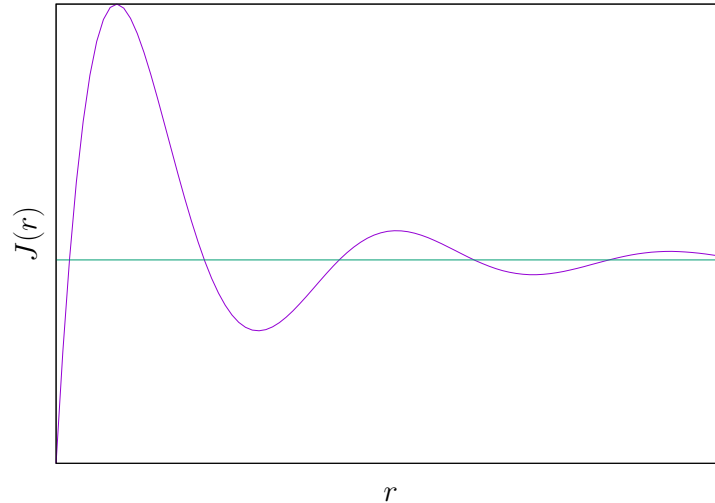


Fig. 1. Dependence of coupling $J(r)$ on distance in the RKKY interaction. Notice the decay with distance, and most important fact, the oscillatory behavior, which induces frustration.

However, some results obtained in experiments performed on films by the Texas group using Heisenberg spin glasses (as CuMn)^{22–27} have been confronted with numerical results simulating Ising spins showing a very good quantitative agreement.^{28–30}

The previous discussion allows us to write the following Edwards-Anderson Hamiltonian which describes the Ising spin glass in a magnetic field h ^{1,15,31}

$$\mathcal{H}_J = - \sum_{i,j} J_{ij} s_i s_j + h \sum_i s_i, \quad (2)$$

where the *quenched* stochastic variables (J_{ij}) can be drawn from a bimodal distribution or from a Gaussian one, both with zero mean and unit variance and $s_i = \pm 1$ are Ising spins. In finite dimensional Ising spin glasses the sum is restricted over all pairs of nearest neighbors, and will be denoted as $\sum_{\langle ij \rangle}$. In this way, the Edwards-Anderson Hamiltonian takes into account the oscillatory behavior of the interaction in the RKKY theory.^{1,15}

Considering that the disorder is quenched, one needs to compute the free energy of the system, from which we can derive the full thermodynamic of the model, in a two step procedure.

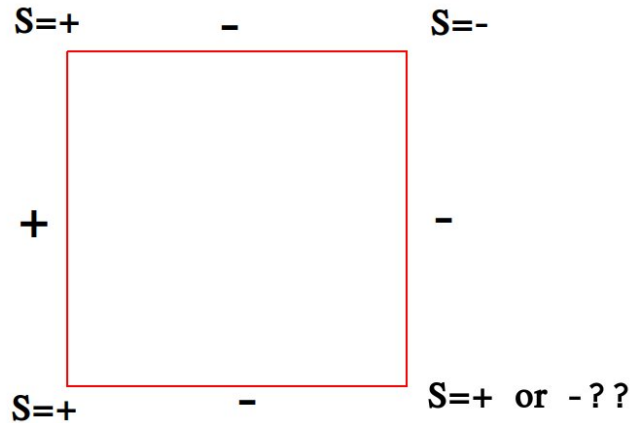


Fig. 2. Frustrated square. For a given choice of couplings (living on the links and their product being negative) and starting with $S = 1$ for the top left spin, the value of the spin lying on the bottom right corner can be $+1$ or -1 . Both values minimize the energy: frustration, the system has two options with the same “cost”.

First, we compute the free energy for a given instance, F_J (realization or sample) of the disorder,

$$F_J = -\frac{1}{\beta} \log Z_J, \quad (3)$$

with $\beta \equiv 1/(k_B T)$, where the partition function Z_J for a given disorder realization is given by

$$Z_J = \sum_{[s]} \exp(-\beta \mathcal{H}_J), \quad (4)$$

where $\sum_{[s]}$ denotes the trace on all the spins.

Second, we take the average of the free energy (of a disorder instance) over the whole set of instances, distributed with the probability density function $p[J]$:

$$F = \int d[J] p[J] F_J, \quad (5)$$

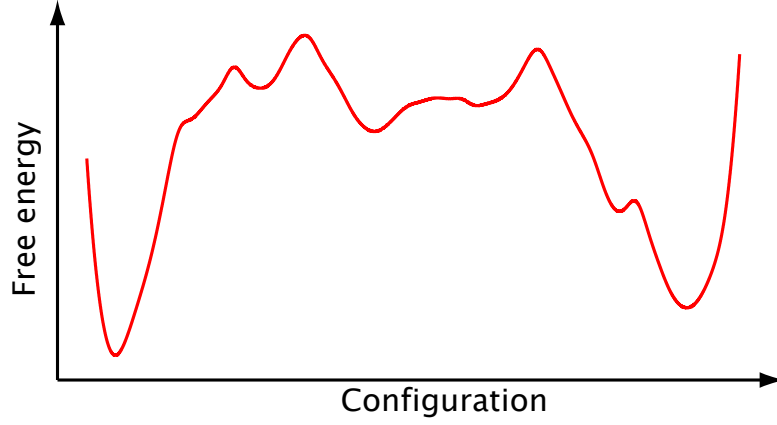


Fig. 3. Free energy landscape for a spin glass: notice the large number of minima, absolute and relative, and the diversity of free energy barriers separating them.

with

$$d[J] \equiv \prod_{i<j} dJ_{ij}, \quad (6)$$

$$p[J] = \exp\left(-\frac{1}{2}N \sum_{i<j} J_{ij}^2\right), \quad (7)$$

N being the number of spins.

Notice that we need to take the average of a logarithm. This fact introduces strong technical difficulties in the analytical solution of the model.

At this point, we can describe what is the spin glass order. In a spin glass phase, all possible staggered magnetizations

$$m_{\mathbf{p}} = \frac{1}{N} \sum_j e^{i\mathbf{p}r_j} \langle s_j \rangle \quad (8)$$

vanish (for all the momenta \mathbf{p}), including the standard one ($\mathbf{p} = 0$). Moreover $s_j \equiv s_{r_j}$. Despite this fact, a spin glass phase presents a non zero *local* magnetization $\langle s_i \rangle \neq 0$.

The order parameter q , the overlap, is then

$$q^J = \frac{1}{N} \sum_i \langle s_i \rangle^2, \quad (9)$$

$$q = \overline{q^J}, \quad (10)$$

where $\langle(\dots)\rangle$ is the thermal average (fixed disorder) and $\overline{(\dots)}$ is the disorder average. The overlap q is zero in the paramagnetic phase and takes a non zero value below the phase transition, in the spin glass phase.

In a numerical simulation is easy to compute the overlap: we simulate in parallel two non-interacting replicas of the system, $\{s_i^{(1)}\}$ and $\{s_i^{(2)}\}$, in presence of the same disorder. Notice that

$$\langle s_i^{(1)} s_i^{(2)} \rangle = \langle s_i^{(1)} \rangle \langle s_i^{(2)} \rangle = \langle s_i^{(1)} \rangle^2, \quad (11)$$

for a given disorder realization. The total overlap per spin is defined as

$$q^{12} = \frac{1}{N} \sum_i q_i^{12}, \quad (12)$$

where

$$q_i^{12} = s_i^{(1)} s_i^{(2)}, \quad (13)$$

and we can compute the probability density function associated with this observable

$$P_J(q) = \langle \delta(q - q^{12}) \rangle, \quad (14)$$

and the probability distribution averaged over the disorder

$$P(q) = \int d[J] p[J] P_J(q) = \overline{P_J(q)}. \quad (15)$$

It is easy to show that

$$q = \int dq' q' P(q'). \quad (16)$$

However, the overlap cannot be measured in experiments where the critical behavior of the material is extracted via the non-linear susceptibility ($\partial^4 f / \partial h^4$) which is proportional to the spin glass susceptibility defined as

$$\chi_{SG} = N \overline{\langle (q^{12})^2 \rangle}. \quad (17)$$

To study spin glass phases with several pure states or phases due to broken ergodicity,¹⁸ see Sec. 3.6 for more details, we need to generalize the above defined overlap by means:

$$q_{\alpha\beta}^J = \frac{1}{N} \sum_i \langle s_i \rangle_\alpha \langle s_i \rangle_\beta, \quad (18)$$

$$q_{\alpha\beta} = \overline{q_{\alpha\beta}^J}, \quad (19)$$

where α and β are two different pure states and $\langle(\dots)\rangle_\gamma$ denotes the thermal average restricted to the state γ . In general, it is possible to write $\langle(\dots)\rangle =$

$\sum_{\alpha} \langle (\dots) \rangle_{\alpha}$ with $\sum_{\alpha} w_{\alpha} = 1$, where the sum runs over all the pure states, and then one can write

$$P_J(q) = \sum_{\alpha\beta} w_{\alpha} w_{\beta} \delta(q - q_{\alpha\beta}^J). \quad (20)$$

The Edwards-Anderson overlap, the maximum possible overlap in the system, is just the maximum overlap: $q_{\alpha\alpha}$.

Despite the fact the magnetic interaction plays an important role in spin glasses, there have been found materials, with a spin glass behavior, where the magnetism is not present. For example, it is possible to study dipolar and quadrupolar spin glasses, where the role of magnetization is played by the polarization vector.^{1,15}

Finally, it is interesting to report the existence of mathematical problems, not related with physics, which present a behavior similar to the one of spin glasses. We can mention optimization problems as the traveling salesman problem, neural networks and biological evolution.^{1,32}

3. Some theoretical results

In this section we discuss different analytical approaches to tackle spin glass behavior. We start with the mean-field approximation, which is exact in infinite dimensions, and then we study finite dimensional spin glasses by presenting the droplet model and the approach based on field theory.

3.1. Mean-field solution

Let us summarize the solution of the Edwards-Anderson model (for $h = 0$) in the mean-field approximation, the so-called Sherrington-Kirpatrick model.³³ The starting point is to use the replica trick. In this trick we replace the logarithm entering the quenched average by the following limit^{32,34}

$$\log x = \lim_{n \rightarrow 0} \frac{x^n - 1}{n}. \quad (21)$$

Applying this trick to the computation of the quenched free energy we obtain

$$\log Z_J = \lim_{n \rightarrow 0} \frac{Z_J^n - 1}{n}. \quad (22)$$

The average on the disorder of the partition function of n non-interacting replicas, $\{s_i^a\}$ ($a = 1, \dots, n$), can be written as

$$Z_n = \overline{Z_J^n} = \sum_{\{s^a\}} \int d[J] \exp\left(\beta \sum_{a=1}^n \sum_{i < j} J_{ij} s_i^a s_j^a - \frac{1}{2} N \sum_{i < j} J_{ij}^2\right). \quad (23)$$

Now, we can compute the integral on the disorder, getting

$$Z_n = \sum_{\{s^a\}} \exp \left[\frac{1}{4} \beta^2 N n + \frac{1}{2} \beta^2 N \sum_{a < b}^n \left(\frac{1}{N} \sum_i s_i^a s_i^b \right)^2 \right]. \quad (24)$$

At this point, we can define a first effective Hamiltonian via

$$Z_n \propto \sum_{\{s^a\}} \exp(-\beta \mathcal{H}_{\text{eff}}\{s_i^a\}), \quad (25)$$

with

$$\mathcal{H}_{\text{eff}}\{s_i^a\} \equiv -\frac{1}{2} \beta N \sum_{a < b}^n \left(\frac{1}{N} \sum_i s_i^a s_i^b \right)^2. \quad (26)$$

This effective Hamiltonian depends on all the replicas $\{s_i^a\}$ with $i = 1, \dots, N$ and $a = 1, \dots, n$. At this point, the disorder has been integrated out.

The quadratic term in the exponential can be made linear by using the Hubbard-Stratonovich trick at the price to introduce the replica matrix Q_{ab}

$$Z_n = \int d[Q] \sum_{\{s^a\}} \exp \left[\frac{1}{4} \beta^2 N n - \frac{1}{2} \beta^2 N \sum_{a < b}^n Q_{ab}^2 + \beta^2 \sum_{a < b}^n \sum_i Q_{ab} s_i^a s_i^b \right]. \quad (27)$$

with

$$d[Q] \equiv \prod_{a < b} dQ_{ab}, \quad (28)$$

In this way we can write the second effective Hamiltonian

$$Z_n = \int d[Q_{ab}] e^{-\mathcal{H}_n\{Q_{ab}\}}, \quad (29)$$

where

$$\mathcal{H}_n\{Q_{ab}\} = -\frac{Nn}{4} \beta^2 + \frac{N}{2} \beta^2 \sum_{a < b} Q_{ab}^2 - N \log \left[\sum_{\{S^a\}} \exp \left(\beta^2 \sum_{a < b} Q_{ab} S^a S^b \right) \right], \quad (30)$$

where $S^a = \pm 1$ are Ising spins. This Hamiltonian depends only on the overlap matrix.

Taking into account that the argument of the exponential is proportional to the number of spins, N , we can compute Z_n using the saddle point method. The stationary condition is

$$\frac{\delta \mathcal{H}_n}{\delta Q_{ab}} = 0, \quad (31)$$

that can be written as

$$Q_{ab} = \langle S^a S^b \rangle_Q, \quad a \neq b, \quad (32)$$

where

$$\langle S^a S^b \rangle_Q \equiv \lim_{n \rightarrow 0} \frac{\sum_{\{S^a\}} S^a S^b \exp(\beta^2 \sum_{a < b} Q_{ab} S^a S^b)}{\sum_{\{S^a\}} \exp(\beta^2 \sum_{a < b} Q_{ab} S^a S^b)}. \quad (33)$$

Furthermore, $\langle S^a S^b \rangle_Q = \lim_{n \rightarrow 0} \langle s_i^a s_i^b \rangle_{\mathcal{H}_{\text{eff}}}$.

At this stage of the analytical computation, we need to do some hypotheses on the structure of the matrix Q . The simplest Ansatz, called 0-step, is³²

$$Q_{ab} = (1 - \delta_{ab})q, \quad (34)$$

where q can be computed in a self-consistent way using the saddle point equation (Eq. 32).

However, this solution leads to two main problems. The first one is that the 0-step solution does not provide with the correct value of the energy and the second one, is that the entropy of this solution is negative. We can try to understand these problems in the framework of field theory.

The effective Hamiltonian can be developed in powers of matrix Q following the framework of the Landau theory of phase transitions. This effective Hamiltonian describes the physics near the critical point.³⁵ For this analysis it is enough to keep terms up to the fourth order in the matrix Q . At this order the effective Hamiltonian is

$$\mathcal{H}_n = \int d^D x \left[(\partial_\mu Q_{ab})^2 + \tau \text{Tr} Q^2 + g_3 \text{Tr} Q^3 + g_4 \text{Tr} Q^4 + \lambda \sum Q_{ab}^4 \right]. \quad (35)$$

If $\lambda = 0$ the symmetry group of this Hamiltonian is $O(n)$. Although, the symmetry group is reduced to the symmetry group S_n (permutations of n elements) as $\lambda \neq 0$.

Now, let us consider again the $\lambda = 0$ case. The 0-step choice for Q_{ab} spontaneously breaks the $O(n)$ symmetry and Goldstone bosons³⁶ (particles or excitations of zero mass) will appear. By turning on the λ coupling, the group $O(n)$ is broken explicitly and the Goldstone bosons are no longer massless (a detailed computation shows that the mass is negative), which clearly indicates that the 0-step solution is unstable.^{32,36-38}

Hence, one needs to find different solutions to that of the 0-step to parameterize the overlap matrix Q_{ab} . G. Parisi³⁹⁻⁴⁴ proposed a general Ansatz for the matrix Q_{ab} which breaks the original $n \times n$ matrix in boxes and the boxes in sub-boxes and so on, in an infinite number of steps.

For example, in Fig. 4 is shown the 2-step level of the Parisi solution (which has infinite levels). At this 2-step level three real values of the overlap q appear: q_0 , q_1 and q_2 and two integer numbers which determine the size of the sub-matrices (box and sub-box), m_1 and m_2 , such that $0 < m_2 < m_1 < n$. Notice that m_2 must divide m_1 and m_1 must divide n .³²

Fig. 4. 2-step of the overlap matrix Q_{ab} . Notice that the matrix has been broken into two main submatrices of sizes m_1 and m_2 , taking values q_0 , q_1 and q_2 . From Ref. [45].

This scheme can be generalized, assuming that n , the number of replicas, is large enough to allow a k -step level of breaking the symmetry of the replicas, where k could be arbitrarily large. Finally, we need to do an analytic continuation to $n = 0$ (to comply with the replica trick).

Given matrix Q_{ab} with the Parisi breaking scheme, one can compute what is the probability to find a given value of q , denoted as $p(q)$, assuming that all the matrix elements have the same probability:³²

$$\begin{aligned} p(q) &= \frac{1}{n(n-1)} \sum_{a \neq b} \delta(Q_{ab} - q) \\ &= \frac{n}{n(n-1)} [(n - m_1)\delta(q - q_0) + (m_1 - m_2)\delta(q - q_1) \\ &\quad + (m_2 - m_3)\delta(q - q_2) + \dots], \end{aligned} \quad (36)$$

with $n > m_1 > m_2 > \dots > 1$.

Taking the limit $n \rightarrow 0$,³² one obtains,

$$p(q) = m_1\delta(q - q_0) + (m_2 - m_1)\delta(q - q_1) + (m_3 - m_2)\delta(q - q_2) + \dots \quad (37)$$

Notice that $p(q)$ is a probability density function composed by sum of Dirac's deltas with different weights, hence, all these weights must be positive and so $0 < m_1 < m_2 < \dots < 1$. Notice that the limiting process ($n \rightarrow 0$) has inverted the order of the different m 's.

At this point we can connect $p(q)$ with the pdf of the overlap defined in Eq. (15), denoted as $P(q)$.

The overlap defined in Eqs. (9) and (10) can be written in the framework of the replica theory as ($a \neq b$)

$$q = \overline{\langle s_i \rangle^2} = \overline{\langle s_i^a s_i^b \rangle} = \left[\frac{\sum_{\{s^a, s^b\}} s_i^a s_i^b \exp(-\beta \sum_{k < l} J_{kl} (s_k^a s_l^a + s_k^b s_l^b))}{\sum_{\{s^a, s^b\}} \exp(-\beta \sum_{k < l} J_{kl} (s_k^a s_l^a + s_k^b s_l^b))} \right]. \quad (38)$$

Notice that the denominator, inside the average over the disorder, is just Z_J^2 . We can introduce $n - 2$ extra factors Z_J in both numerator and denominator, obtaining in the limit $n \rightarrow 0$ (the final Z_J^n in the denominator goes to one):¹⁸

$$q = \overline{\langle s_i \rangle^2} = \lim_{n \rightarrow 0} \sum_{\{s^a\}} s_i^a s_i^b \exp(-\beta \mathcal{H}_{\text{eff}}\{s_i^a\}) \quad (39)$$

$$= \lim_{n \rightarrow 0} \frac{\sum_{\{s^a\}} s_i^a s_i^b \exp(-\beta \mathcal{H}_{\text{eff}}\{s_i^a\})}{\sum_{\{s^a\}} \exp(-\beta \mathcal{H}_{\text{eff}}\{s_i^a\})} = \lim_{n \rightarrow 0} \langle s_i^a s_i^b \rangle_{\mathcal{H}_{\text{eff}}} \quad (40)$$

$$= \langle S^a S^b \rangle_Q = \lim_{n \rightarrow 0} \frac{1}{n(n-1)} \sum_{a \neq b} Q_{ab}, \quad (41)$$

where, in the last equation, we must average over all the saddle-point solutions (we also refer to the analytical computations we have done to transform Eq. (27) into Eq. (30)). In particular, in Eq. (40), we have used that in Eq. (25) $Z_n \rightarrow 1$ as $n \rightarrow 0$.

Hence $p(q)$ and $P(q)$ have the same first momentum. It is possible to generalize this computation and to show that $p(q) = P(q)$.³² In the rest of this book chapter we will denote the pdf of the overlap as $P(q)$.

We continue by studying the properties of $P(q)$. It is possible to show that in the limit of an infinite number of breakings (full replica symmetry breaking, RSB) the real parameters q_k become a continuous function $q_k \rightarrow q(x)$, with $x \in [0, 1]$ and that the function $x(q)$ (inverse of $q(x)$) is related with $P(q)$ via³²

$$\frac{dx}{dq} = P(q). \quad (42)$$

Before finishing this section we summarize some of the most important physical and mathematical properties of the Parisi solution:^{32,34,39-44,46-51}

- It is exact in infinite dimensions. This has rigorously been shown in Refs. [52–54].
- It shows an infinite number of pure states not related by any symmetry.
- These infinite pure states are organized in a ultrametric way⁵⁵. We can recall at this point, the definition of an ultrametric space. A space is ultrametric if all the triplets of elements belonging to this space (A, B, C) satisfy the ultrametric inequality:

$$d(A; B) \leq \max(d(A, C), d(B, C)).$$

In spin glasses we can introduce a distance by using the overlaps (now the elements of this space are the pure states, see Sec. 3.6)

$$d(\alpha, \beta) = \frac{1}{2} (q_{EA} - q_{\alpha\beta}). \quad (43)$$

In Fig. 5 we have drawn the ultrametric organization of the pure states: the end of the leaves are the pure states, having q_{EA} as their overlap.

- The spin glass phase is stable under small magnetic fields. A transition line in the temperature-magnetic field plane separates a paramagnetic phase from a spin glass one (the de Almeida-Thouless line⁵⁶).
- The excitations of the ground state are space filling, i.e. the dimension of the excitations is just that of the space, D .
- Overlap equivalence. All the possible definitions of the overlap, e.g. spin overlap or link overlap, provide the same information on the physical properties of the system. For example the link overlap is defined as

$$q_l = \frac{1}{ND} \sum_{\langle ij \rangle} s_i^{(1)} s_j^{(1)} s_i^{(2)} s_j^{(2)}, \quad (44)$$

where $\{s_i^1\}$ and $\{s_i^2\}$ are two real replicas and $\sum_{\langle ij \rangle}$ denotes sum over all pairs of nearest neighbors. In the SK model, one can show that $q_l = q^2$.

- Stochastic stability. The Hamiltonian of spin glasses is *generic* against random perturbations.

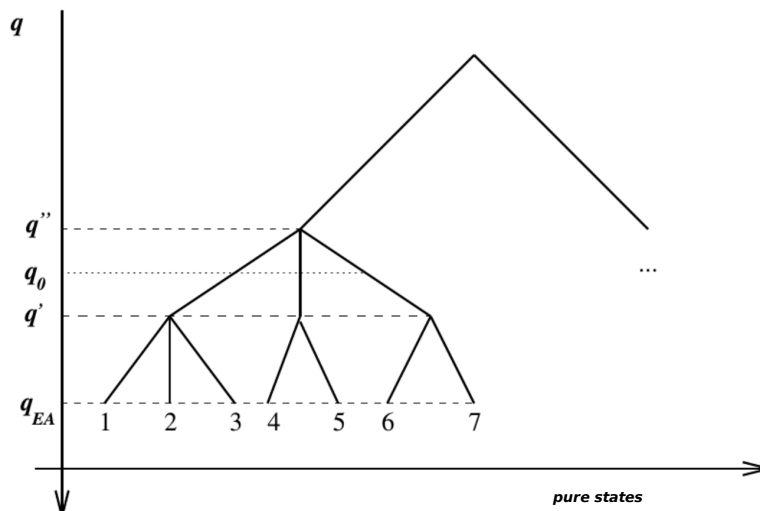


Fig. 5. Ultrametric organization of the pure states in the Parisi solution.

3.2. Spin glasses in finite dimensions

Once we have characterized the behavior of spin glasses in infinite dimensions, the fully connected model, we want to understand what are the properties of spin glasses in finite dimensions. Different theories have been developed to describe the behavior of spin glass in finite dimensions. Hereafter, in the next three sections, we report the two most important approaches: the droplet model and the RSB theory.

3.3. The droplet model

The droplet theory predicts that the spin glasses above the lower critical dimension (D_l) show only two pure states in the spin glass phase and the behavior of this spin glass phase is determined by compact excitations on the ground state. The droplet model can be formulated in terms of the Migdal-Kadanoff approximation of the renormalization group^{57,58} (which is exact in $D = 1$)^{59,60} or by means a phenomenological theory,^{18,61–64} both approaches being equivalent.

The most important properties of this phenomenological theory are:

- The droplets are compact excitations with fractal dimension D_F . The energy of a droplet of linear dimension L grows as L^θ with

$$\theta < (D - 1)/2 < D - 1 < D_F < D.$$

- In the dynamics, the free energy barriers behave as L^ψ , with $\psi \geq \theta$.
- The spin glass phase is unstable against the presence of a magnetic field.
- There are two pure states (related by spin flip), and thus, the probability distribution of the overlap is trivial: sum of two Dirac's deltas.

Finally, there is a variation of the droplet model, known as the chaotic pairs model. In this picture the system has two pure states (as in the droplet model), but these two states vary chaotically with the size of the system, see Sec. 3.6.

3.4. Field theory ($h = 0$)

In this section, we address the problem of how to build a field theory using the RSB solution as starting point in absence of a magnetic field. For a theoretical description of the theory in presence of a magnetic field, see Sec. 3.5.

We start considering the theory in infinite dimensions (using the mean-field approximation, which is exact in $D = \infty$). Next, the upper critical dimension D_u is computed. Above it, the predictions of the mean-field approximation hold and below, infrared divergences appear and we need to resort to the renormalization group to tackle them.³⁵⁻³⁸

This is the standard approach and it has been applied (with a huge success) in the study of a large number of models, for example, the Ising model or models with $O(N)$ symmetry.

The upper critical dimension is determined by the dimension of the cubic coupling, g_3 , in the effective Hamiltonian, see Eq. (35), and it turns to be $D_u = 6$. Below the upper critical dimension τ and g_3 are the relevant parameters (using the terminology of the renormalization group³⁵) and g_4 and λ are irrelevant, hence, we need to study the field theory of a ϕ^3 theory with tensor couplings. By using this theory, it is possible to compute analytically the critical exponents using the ϵ -expansion (where $\epsilon = 6 - D$), see Refs. [18,65–67]. Moreover, by using this theoretical framework, it has been possible to compute the logarithmic corrections at the upper critical dimension in these models, see Refs. [68–72].

To complete this discussion, let us remark that the lower critical dimensions in absence of a magnetic field seems to be $D_l = 2.5$.⁷³⁻⁷⁵ This issue has been studied experimentally by studying spin glasses in film geometries,

finding a strong evidence that $2 < D_l < 3$.²²⁻²⁵

The low temperature spin glass phase is critical (in this model the $T = 0$ critical point has infinite correlation length, as in the $O(N)$ model, $N > 1$, $D > 2$) and to perform a field theoretical analysis we also need to consider the g_4 and λ couplings. The mean field solution, on which is based this approach, is very complicated mathematically, as we have shown in Sec. 3.1. These computations have been partially performed^{17,76,77} and the behavior of the different correlation functions (propagators) which depend on the overlap q was obtained. All the connected correlation functions present an algebraic decay (since the low temperature is critical) as in the droplet model.

Thereupon, we summarize the main results.^{17,76,77} Firstly, we define the (connected) correlation function

$$C_4(\mathbf{r}|q) \equiv \frac{1}{V} \sum_{\mathbf{x}} \overline{\langle s_{\mathbf{x}}^{(1)} s_{\mathbf{x}+\mathbf{r}}^{(1)} s_{\mathbf{x}}^{(2)} s_{\mathbf{x}+\mathbf{r}}^{(2)} \rangle}. \quad (45)$$

$\langle \dots \rangle$ denotes the thermal average, $\overline{\langle \dots \rangle}$ is the average over the disorder, V is the volume of the system, $\{s_i^{(1)}\}$ and $\{s_i^{(2)}\}$ are, as usual, two non-interacting real copies of the system (real replicas) and the system is constrained to have a fixed overlap q

$$q = \frac{1}{V} \sum_{\mathbf{x}} \overline{\langle s_{\mathbf{x}}^{(1)} s_{\mathbf{x}}^{(2)} \rangle}. \quad (46)$$

This conditional correlation function decays algebraically as

$$C_4(\mathbf{r}|q) \simeq q^2 + \frac{A(q)}{r^{\theta(q)}}. \quad (47)$$

The following values for the exponent $\theta(q)$ were obtained:^{17,51,76,77}

- $\theta(q_{\text{EA}}) = D - 2$. This results could be exact, a sort of Goldstone theorem.
- $\theta(q) = D - 3$ para $q_{\text{EA}} > q > 0$. This exponent could be modified below $D_u = 6$.
- $\theta(q_m) = D - 4$ for the smallest overlap $q_m = 0$. This mode is called replicon.

The full (non-constrained) correlation function can be recovered with the help of $P(q)$, the probability to find a given overlap q , see Eq. (37), as

$$C_4(r) = \int dq P(q) C_4(r|q). \quad (48)$$

We can refer that the prediction of the droplet model is

$$C_4(r) \simeq q_{\text{EA}}^2 + \frac{A}{r^\theta}, \quad (49)$$

where θ is the exponent which controls the thermal excitations of the system (see Sec. 3.3).

In the droplet model there is only one correlation function since there is only a pure state having an equilibrium overlap q_{EA} , see Sec. 3.3, whereas in the RSB theory it is possible to find two states with overlap in the interval $[0, q_{\text{EA}}]$, and therefore it is possible to obtain a correlation function in which one replica belongs to the state α and the other to the β one having mutual overlap $q_{\alpha\beta} = q$, measuring $C_4(r|q)$.

Finally, let us remark that it is possible to show in a rigorous way that if the spin glasses in finite dimensions present ultrametricity, the mathematical properties of this ultrametricity are the same as of the ultrametricity found in the Parisi theory (RSB) which holds in infinite dimensions.⁷⁸

Furthermore, stochastic stability and replica equivalence or overlap equivalence imply ultrametricity⁷⁹ and numerical simulations have provided strong numerical support for both stochastic stability and overlap equivalence in three dimensional spin glasses.^{80–84}

3.5. Field theory ($h \neq 0$)

The analytical study of spin glasses in presence of a magnetic field below its upper critical dimensions has been and still is a challenge. In Fig. 6 we show the renormalization group flow for spin glasses below the upper critical dimension and in presence of a magnetic field assuming RSB or droplet. Despite all the difficulties, the following facts are known:

- The upper critical dimensions is 6.⁸⁶
- Due to the appearance of a dangerous irrelevant variable the critical exponents for some observables change already in $D = 8$.⁶¹
- One can project the full theory on its most divergent components. Working with this projected theory⁸⁷ no fixed points were found at the first order in perturbation theory. The no existence of fixed point of the renormalization group in a theory is usually interpreted as

- (1) it is needed to work at higher order in perturbation theory in order to find it (or them);⁸⁸
- (2) the fixed point is of non-perturbative nature and one needs to resort to non-perturbative methods;⁸⁹

- (3) the phase transition is first-order (runaway trajectories).
- By using the most general Hamiltonian in the replica symmetric phase and by relaxing the replica trick condition $n = 0$, a fixed point below six dimensions was found.⁹⁰
 - In Refs. [91,92] the de Almeida-Thouless transition was found below the upper critical dimension ($D_U = 6$) using analytical prolongation.

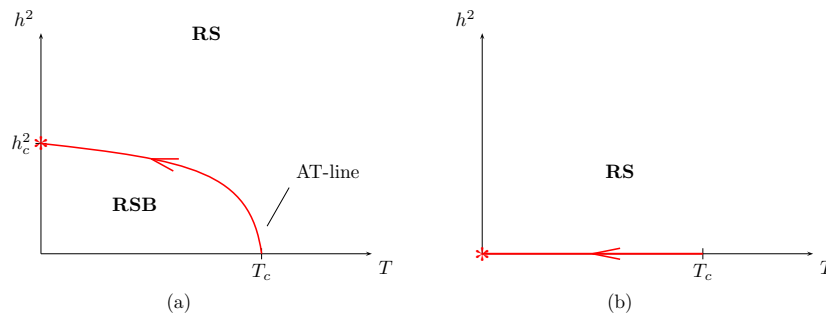


Fig. 6. Renormalization group flow for spin glasses in presence of a magnetic field for dimension $D_l < D < D_u$.⁹² On the left panel, we show the flow assuming replica symmetry breaking (phase transition in field). On the right the renormalization group flow assuming the spin glass phase is unstable under magnetic field (droplet model). The fixed points of the renormalization group equations for temperature and magnetic field are marked with a star. The continuous lines, with an arrow, mark the critical surfaces, in which the correlation length is infinite, and the arrows point to the directions in which the flow is moving as the scale (in space) of the renormalization group transformation grows.

Finally, in Ref. [93] analytical computations were performed suggesting the possible existence of a quasi-first-order phase transition below the upper critical dimension.

3.6. Metastate

Pure phases (or pure states) are macroscopic homogeneous states of matter, for example, liquid, gaseous and solid phases. In principle, it is not difficult to determine if a lump of matter is in a given phase or not. However, to define states in the thermodynamic limit (infinite volume) is not easy.

Rigorously, a state is a probability distribution and with it we can compute averages: hence, we can see this probability distribution as a linear

functional.⁹⁴

For example, in the two dimensional Ising model (with no disorder) one can define three (states) phases: paramagnetic, ferromagnetic (with positive magnetization) and ferromagnetic (with negative magnetization) phase. The two ferromagnetic phases can be defined using the following limits

$$\langle(\dots)\rangle_+ = \lim_{h \rightarrow 0^+} \lim_{L \rightarrow \infty} \langle(\dots)\rangle_{(L,h)}, \quad (50)$$

$$\langle(\dots)\rangle_- = \lim_{h \rightarrow 0^-} \lim_{L \rightarrow \infty} \langle(\dots)\rangle_{(L,h)}. \quad (51)$$

In general, both in experiments and in numerical simulations, we obtain mixed states: i.e. numerical configurations or lumps with interfaces which split different pure states (or pure phases). These mixed states form a convex set in which its extremal points define the pure states. The mixed states can be written in terms of pure states in the following way (we particularize for the Ising model above one dimension and below the critical temperature):

$$\langle(\dots)\rangle = w \langle(\dots)\rangle_+ + (1-w) \langle(\dots)\rangle_-, \quad (52)$$

where $0 < w < 1$ is the proportion of the positive magnetization phase.

In a more general way, one can write an expression of a given state Γ in terms of pure states Γ_α

$$\Gamma = \sum_{\alpha} w_{\alpha} \Gamma_{\alpha}, \quad (53)$$

with $\sum_{\alpha} w_{\alpha} = 1$, $w_{\alpha} > 0$ and the sum runs over all the pure states. Another important property of pure states is that intensive magnitudes do not fluctuate.

The generalization of the previous concepts and mathematical tools to systems with quenched disorder is very complicated, since the sequence of states $\Gamma_{L,J}$, J denotes the quenched disorder, usually does not converge (chaotic dependence on system size).^{16,95}

Some models in which the sequence of states does not converge are:⁵¹

- (1) Ising model ($D > 1$) without disorder with spins on the fixed boundary conditions which change as it changes the size of the system.
- (2) Ising model ($D > 2$) in presence of a random magnetic field with zero mean and unit variance. The magnetization of the ferromagnetic phase does not converge since it is given by the sign of $\sum_i h_i$, which is a stochastic variable.

- (3) Ising spin glasses in the chaotic pairs scenario. For each size the system presents two pure states (related by a global spin flip symmetry), however, these two states vary in a chaotic way as the lattice size grows.^{96–98}

The concept of metastate was introduced to tackle the intrinsic lack of convergence that show these models.^{96–98} Despite the lack of convergence of the sequence $\Gamma_{L,J}$, it is possible to compute the frequency a given state appears in that sequence as $L \rightarrow \infty$. The set of these frequencies defines the Newman-Stein metastate.

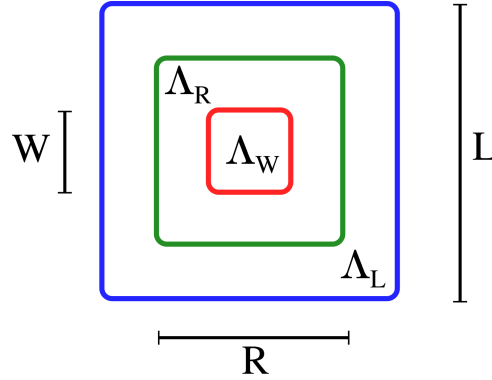


Fig. 7. Construction of the Aizenman-Wehr metastate. Notice the different boxes (squares in the figure) defined in order to compute the metastate.⁹⁹

Before the introduction of the Newman-Stein metastate, another definition of the metastate was given by Aizenman and Wehr.¹⁰⁰ Although, a proof of the equivalence of both metastates is still lacking.

The definition of the Aizenman-Wehr allows for a numerical implementation. The construction of the Aizenman-Wehr is as follows:

- (1) For simplicity, let us consider a two-dimensional system, see Fig. 7. In this figure we draw three different regions: Λ_W , Λ_R and Λ_L .
- (2) We call the disorder inside the inner region Λ_R , inner disorder, denoted as \mathcal{I} .
- (3) The disorder in the outer region $\Lambda_L \setminus \Lambda_R$ is called an outer disorder and denoted as \mathcal{O} .
- (4) The measurements will be done in the region Λ_W . To avoid influences of the transition region between the inner and outer regions, we will try to implement the limit $\Lambda_W \ll \Lambda_R \ll \Lambda_L$.

In this framework we are interested to compute the following limit

$$\kappa_{\mathcal{I},R}(\Gamma) = \lim_{L \rightarrow \infty} \mathbb{E}_{\mathcal{O}} \left[\delta^{(F)}(\Gamma - \Gamma_{L,J}) \right], \quad (54)$$

where $\mathbb{E}_{\mathcal{O}}[\dots]$ denotes the average over the outer disorder.

Assuming that the following limit exists

$$\kappa(\Gamma) = \lim_{R \rightarrow \infty} \kappa_{\mathcal{I},R}(\Gamma), \quad (55)$$

then it will not depend on the inner disorder \mathcal{I} and will provide us the Aizenman-Wehr metastate.

We can compute averages over the metastate by using

$$\langle \dots \rangle_{\rho} \equiv [\langle \dots \rangle_{\Gamma}]_{\kappa}. \quad (56)$$

Therefore, the metastate is also a state.

To characterize the metastate, it is very useful to compute the following correlation function

$$C_{\rho}(x) = \overline{[\langle s_{\mathbf{0}} s_{\mathbf{x}} \rangle_{\Gamma}]_{\kappa}^2} \sim |x|^{-(D-\zeta)}, \quad (57)$$

where ζ is a new exponent introduced by Read.¹⁰¹

The ζ -exponent provides important information about the structure of the states of the spin glass phase:

- $\log \mathcal{N}_{\text{states}}(W) \sim W^{D-\zeta}$ (with $\zeta \geq 1$). Where $\mathcal{N}_{\text{states}}(W)$ is the number of states in a system with size W .
- If $\zeta < D$ then metastate is disperse (therefore, the droplet theory does not hold).
- Read conjectured $\zeta = D - \theta(0)$, where, we recall, $\theta(0)$ is the exponent of the replicon mode, see Eq. (47) of Sec. 3.4.¹⁰¹

4. Some numerical results

After the discussion of some aspects of the theories aimed to explain the properties of spin glasses in infinite and finite dimensions, we report in the following sections numerical simulations at equilibrium in presence/absence of the magnetic field.

4.1. Phase transition at $h = 0$

Let us present numerical results showing the existence of a phase transition in the three dimensional Ising spin glass at $h = 0$.

Usually, the numerical simulations are performed using the Monte Carlo exchange method (also known as parallel tempering).^{102–105} Another popular approach in the last years has been the population annealing method.^{106–108}

In this section, we closely follow Ref. [109] where the supercomputer Janus I was used, see Sec. A.2 for a description of the most important characteristic of this computer.

As it has been stated in this chapter, the spin glass order parameter is based on the overlap. In numerical simulations, one can run in parallel different non-interacting real replicas, denoted, as usual, as $s_{\mathbf{x}}^a$. Usually, the number of simulated real replicas is between two and six. We can recall again the general definition of the overlap ($a \neq b$)

$$q_{\mathbf{x}}^{ab} = s_{\mathbf{x}}^a s_{\mathbf{x}}^b. \quad (58)$$

In the simulations reported in this section¹⁰⁹ four copies of the system were simulated with the same disorder (real replicas), therefore, one can compute six different overlaps q^{ab} .

One can define the overlap-overlap correlation function given by

$$G(\mathbf{r}) = \frac{1}{V} \sum_{\mathbf{x}} \langle q_{\mathbf{x}+\mathbf{r}}^{ab} q_{\mathbf{x}}^{ab} \rangle, \quad (59)$$

and finally the total overlap per volume of the system (V)

$$q^{ab} = \frac{1}{V} \sum_{\mathbf{x}} q_{\mathbf{x}}^{ab}. \quad (60)$$

Next, we compute the Fourier transform of the overlap-overlap correlation function

$$\tilde{G}(\mathbf{k}) = \frac{1}{V} \sum_{\mathbf{r}} G(\mathbf{r}) e^{i\mathbf{k}\cdot\mathbf{r}}, \quad (61)$$

which allows us to compute the second-moment correlation length^{36,110}

$$\xi = \frac{1}{2 \sin(k_{\min}/2)} \sqrt{\frac{\tilde{G}(0)}{\tilde{G}(\mathbf{k}_{\min})} - 1}, \quad (62)$$

where $\mathbf{k}_{\min} = (2\pi/L, 0, 0)$ or the other two possible permutations. The total susceptibility is given by the correlation function computed in the Fourier space at zero momentum

$$\chi_{\text{SG}} = \tilde{G}(0) = V \overline{\langle q^2 \rangle}. \quad (63)$$

Finally, the correlation length in units of system size ξ/L is

$$R_{\xi} = \xi/L. \quad (64)$$

We recall that ξ/L is universal at the critical point.

In addition to ξ/L we can define the following observables which also take universal values at the critical point:

$$U_4 = \frac{\langle q^4 \rangle}{\langle q^2 \rangle^2}, \quad (65)$$

$$U_{22} = \frac{\langle q^2 \rangle^2}{\langle q^4 \rangle}, \quad (66)$$

$$U_{111} = \frac{\langle q^{12} q^{23} q^{31} \rangle^{4/3}}{\langle q^4 \rangle}, \quad (67)$$

$$U_{1111} = \frac{\langle q^{12} q^{23} q^{34} q^{41} \rangle}{\langle q^4 \rangle}, \quad (68)$$

$$R_{12} = \frac{\tilde{G}(2\pi/L, 0, 0)}{\tilde{G}(2\pi/L, 2\pi/L, 0)}, \quad (69)$$

$$B_\chi = 3V^2 \frac{\langle |\tilde{q}(2\pi/L, 0, 0)|^4 \rangle}{[\tilde{G}(2\pi/L, 0, 0)]^2}, \quad (70)$$

where

$$\tilde{q}^{ab}(\mathbf{k}) = \frac{1}{V} \sum_{\mathbf{x}} q_{\mathbf{x}}^{ab} e^{i\mathbf{k}\cdot\mathbf{x}}. \quad (71)$$

We show in Fig. 8 the different crossing points of the R_ξ as a function of the temperature and the size of the system. The study of these crossing points by means of the quotient method (see Sec. A.1 for a detailed description of this method) allows to compute the critical exponents and other universal quantities.¹⁰⁹ The results of this analysis can be read in Table 1.¹⁰⁹

In this part of the book chapter, we have only focused on the Ising spin glass with binary couplings. The field theory of Ising spin glass only depends on the first two cumulants of the probability distribution of the couplings: the other (infinite) cumulants of the probability distribution of the couplings J_{ij} only induce irrelevant couplings in the field theory, and following the general theory of the renormalization group,^{35–38,57,58} they only induce scaling corrections without changing the values of the critical exponents (universality). This issue has been checked in Refs. [111–114]. However, some references, see for example Ref. [115], have reported violation of universality in Ising spin glass models.

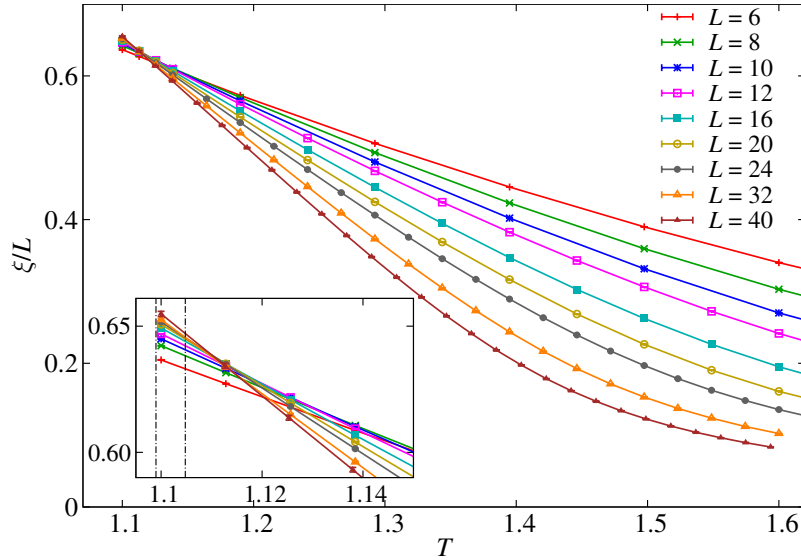


Fig. 8. Behavior of the second-moment correlation length as a function of the temperature for different values of the size of the system. In the inset, we show a zoom of the region in which ξ/L curves cross. We mark with two vertical lines the final value of the critical temperature, and taking into account the statistical error, one can quote: $T_c = 1.1019(29)$.¹⁰⁹

4.2. Behavior of the correlation functions in the spin glass phase

Once we have characterized the critical point, we try to characterize the properties of the low temperature spin glass phase.

Let us consider the conditional spatial correlation function $C_4(r|q)$, see Eq. (45). We focus on the real space behavior of this conditional correlation function, a detailed study of its Fourier transform can be found in Ref. [118].

The first numerical computation of $C_4(r|q = 0)$ was performed in Ref. [116] working in the out-of-equilibrium regime (with an extrapolation to infinite time). Subsequently, this out-of-equilibrium correlation function was confronted with an equilibrium computation of the same observable.¹¹⁷ In Fig. 9 we show these two $C_4(r|q = 0)$ (lower curves of this figure) together with the full correlation one (the upper curve of the figure): notice the very good agreement between the out-of-equilibrium and equilibrium computation of $C_4(r|q = 0)$.

The conditional correlation function $C_4(r|q = 0)$ corresponds with the

Table 1. Summary of the critical exponents and the values (universal) of different cumulants at the critical point.¹⁰⁹

Exponent/Observable
$\omega = 1.12(10)$
$\eta = -0.3900(36)$
$\nu = 2.562(42)$
$R_\xi^* = 0.6516(32)$
$U_4^* = 1.4899(28)$
$\alpha = -5.69(13)$
$\beta = 0.782(10)$
$\gamma = 6.13(11)$
$T_c = 1.1019(29)$
$U_{1111}^* = 0.4714(14)$
$U_{22}^* = 0.7681(16)$
$U_{111}^* = 0.4489(15)$
$B_\chi^* = 2.4142(51)$
$R_{12}^* = 2.211 \pm 0.006$

replicon correlation function in the framework of RSB theory and it should decay algebraically with the exponent $\theta(0)$, see Eq. (47) of Sec. 3.4. This power law decay was corroborated in Refs. [116,117] (see Fig. 9). The replicon exponent was estimated to be $\theta(0) = 0.50(2)$ for the three dimensional Ising spin glass with Gaussian couplings.¹¹⁶

Most recent out-of-equilibrium numerical simulations performed on the Janus I supercomputer have provided with an accurate value of the replicon exponent: $\theta(0) = 0.38(2)$.^{80,118}

In the next paragraphs, we report some results obtained at equilibrium in the three dimensional Ising spin glass model with the help of Janus I. In these numerical simulations, we were able to proceed up to $L \leq 32$ inside the thermalized low temperature phase.⁸¹

First, we study the $q = 0$ sector in which the prediction of the droplet model and the RSB theory are fully different. In left panel of Fig. 10 we show $C_4(r|q = 0)$ for $T = 0.703 \sim 0.7T_c$ which goes to zero for large r . In the right panel of this figure we show the scaling plot of this observable by using the replicon exponent $\theta = 0.38(2)$ and not that predicted by the droplet theory $y = \theta(q_{EA}) = 0.2$.⁵⁹ Note that by using $\theta = 0.38(2)$ the curves collapse (see Fig. 10-left panel).

Second, we consider the rescaled difference of the conditional correlation function evaluated at $r = L/4$ and $r = L/2$, which following RSB should

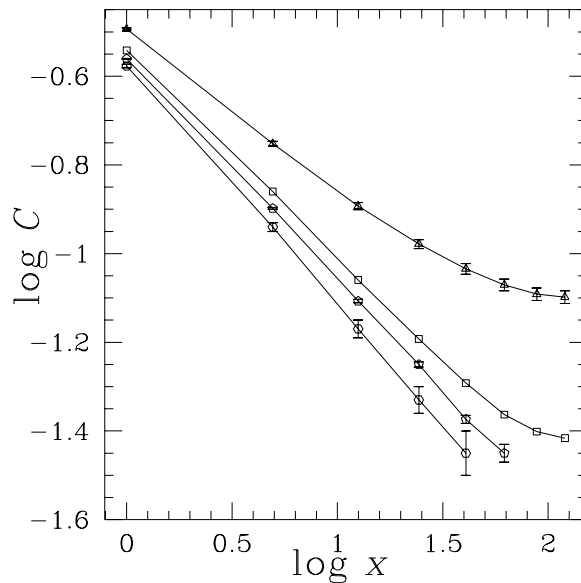


Fig. 9. Conditional overlap-overlap correlation function $C \equiv C_4(x|q)$ for the three-dimensional Ising spin glass with Gaussian couplings. $T = 0.7 \simeq 0.7T_c$. The lower curve is the infinite time extrapolation of the non-equilibrium correlation function $C_4(x|q=0)$ obtained by a sudden quench ($L = 64$). The second curve from the bottom is $C_4(x|q=0)$ obtained by a slow annealing ($L = 64$). The third curve is the equilibrium correlation function computed with the constraint $|q| < 0.01$ ($L = 16$). The upper curve is the full equilibrium correlation function, including all configurations ($L = 16$). From Refs. [116, 117].

behave as (see Eq. (47))

$$L^{\theta(q)} \left(C_4(r = L/4|q) - C_4(r = L/2|q) \right) \sim 1, \quad (72)$$

in order to remove the background, for large distances, in the $C_4(r|q)$ correlation function (finite volume effect). This rescaled difference as a function of q^2 is shown in Fig. 11. Notice that a good scaling was found in the re-

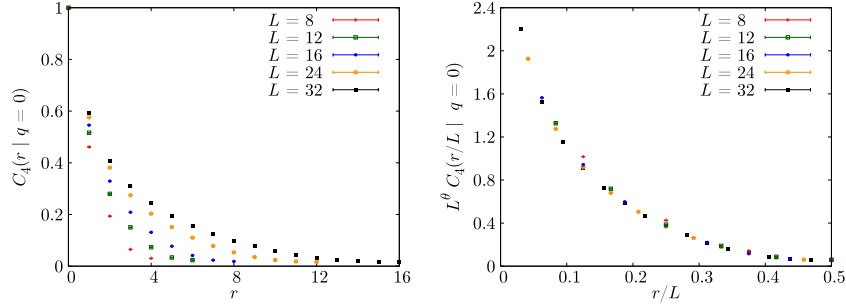


Fig. 10. $C_4(r|q=0)$ versus r for $T = 0.703 \simeq 0.7T_c$ (left panel). We show in the right panel the scaling collapse of $L^{\theta(0)}C_4(r/L|q=0)$ using the replicon exponent $\theta = 0.38$ as a function of r/L .⁸⁰

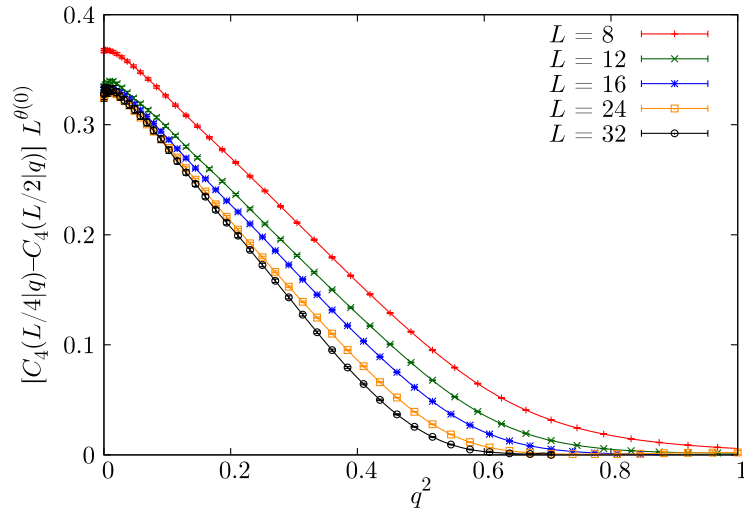


Fig. 11. Rescaled difference of the correlation function, Eq. (72), as function of q^2 . We have used $\theta(0) = 0.38(2)$ from a out-of-equilibrium numerical simulation.⁸⁰

gion $q^2 < 0.2$, this means that the correlation functions $C_4(r|q) - q^2$ decay following a power law in the overlap interval (see also Ref. [119]).

Moreover, for $q^2 > 0.2$, the scaling breaks down pointing to a value of the θ -exponent used to rescale in Eq. (72) that is larger than $\theta(0)$. A detailed analysis¹¹⁸ suggests that $\theta(q_{EA}) \sim 0.6$ and that the crossover between the small and large q^2 can be analyzed using finite size scaling.¹¹⁸

To close this section, we report the final values of these exponents obtained in these numerical simulations at equilibrium: $\theta(0) = 0.377(14)^{81}$ and $\theta(q_{\text{EA}}) \simeq 0.511(16)(60)^{81}$. Finally we quote that an out-of-equilibrium analysis provided $\theta(q_{\text{EA}}) \simeq 0.78(10)^{80,118}$.

4.3. Metastate: Numerical results

In this section, we build numerically the metastate following the Aizenman and Wehr¹⁰⁰ and we present the main results obtained in Ref. [99].

We start with some definitions. The average over the Gibbs state $\langle \dots \rangle_{\Gamma}$ is estimated via Monte Carlo thermal averages $\langle \dots \rangle$ at fixed disorder J .

The average over the metastate is given by

$$[\dots]_{\kappa} = \frac{1}{\mathcal{N}_{\mathcal{O}}} \sum_{\circ} (\dots), \quad (73)$$

and the one over the internal disorder by

$$\overline{(\dots)} = \frac{1}{\mathcal{N}_{\mathcal{I}}} \sum_{\mathbf{i}} (\dots). \quad (74)$$

The indices \mathbf{i} and \circ run over the number of inner and outer disorder realizations, denoted as $\mathcal{N}_{\mathcal{I}}$ and $\mathcal{N}_{\mathcal{O}}$, respectively.

For example, the metastate spin correlation function (see Eq. (57)) can be explicitly computed as

$$\begin{aligned} C_{\rho}(|\mathbf{x}|) &= \overline{[\langle s_{\mathbf{o}} s_{\mathbf{x}} \rangle_{\Gamma}]_{\kappa}^2} \\ &= \frac{1}{\mathcal{N}_{\mathcal{I}}} \sum_{\mathbf{i}} \left(\frac{1}{\mathcal{N}_{\mathcal{O}}} \sum_{\circ} \langle s_{\mathbf{o}}^{\mathbf{i};\circ} s_{\mathbf{x}}^{\mathbf{i};\circ} \rangle \right)^2 \\ &= \frac{1}{\mathcal{N}_{\mathcal{I}}} \sum_{\mathbf{i}} \frac{1}{\mathcal{N}_{\mathcal{O}}^2} \sum_{\circ, \circ'} \langle s_{\mathbf{o}}^{\mathbf{i};\circ} s_{\mathbf{x}}^{\mathbf{i};\circ} s_{\mathbf{o}}^{\mathbf{i};\circ'} s_{\mathbf{x}}^{\mathbf{i};\circ'} \rangle. \end{aligned} \quad (75)$$

Inside Λ_W , see Fig. 7, we can compute a generalized overlap using two non-interacting real replicas (Ising spins), denoted as $\{\sigma\}$ and $\{\tau\}$. These two real replicas share the same disorder, denoted by \mathbf{i} , with different or the same outer disorder, denoted as \circ , for σ , and \circ' , for τ :

$$q_{\mathbf{i};\circ,\circ'} \equiv \frac{1}{W^3} \sum_{\mathbf{x} \in \Lambda_W} \sigma_{\mathbf{x}}^{\mathbf{i};\circ} \tau_{\mathbf{x}}^{\mathbf{i};\circ'}. \quad (76)$$

Notice the possible cases: $\circ = \circ'$ and $\circ \neq \circ'$. Therefore, we can compute the following probability distributions of the generalized overlap $q_{\mathbf{i};\circ,\circ'}$:

$$P_{\mathbf{i}}(q) = \frac{1}{\mathcal{N}_{\mathcal{O}}} \sum_{\circ} \langle \delta(q - q_{\mathbf{i};\circ,\circ}) \rangle, \quad (77)$$

$$P(q) = \frac{1}{\mathcal{N}_{\mathcal{I}}} \sum_{\mathbf{i}} P_{\mathbf{i}}(q), \quad (78)$$

$$P_{\rho, \mathbf{i}}(q) = \frac{1}{\mathcal{N}_{\mathcal{O}}^2} \sum_{o, o'} \langle \delta(q - q_{\mathbf{i}; o, o'}) \rangle, \quad (79)$$

$$P_{\rho}(q) = \frac{1}{\mathcal{N}_{\mathcal{I}}} \sum_{\mathbf{i}} P_{\rho, \mathbf{i}}(q). \quad (80)$$

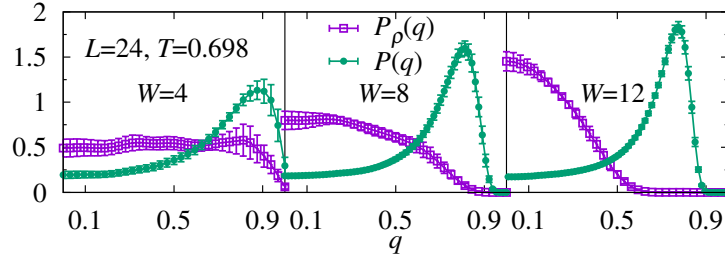


Fig. 12. The overlap probability distributions $P_{\rho}(q)$ and $P(q)$ against the overlap for $L = 24$, $R = L/2$, $T = 0.698$ and for different values of the window size, $W = 4, 8$ and 12 .⁹⁹

$P(q)$ is just the standard overlap probability distribution, but $P_{\rho}(q)$ is the probability distribution of the overlap averaged over the metastate.

Regarding $P_{\rho}(q)$, despite having a trivial limit $P_{\rho}(q) \rightarrow \delta(q)$ for $W \rightarrow \infty$,¹⁰¹ its variance for finite values of W provides with very useful information

$$\chi_{\rho} = \sum_{\mathbf{x} \in \Lambda_W} C_{\rho}(\mathbf{x}) = W^d \int q^2 P_{\rho}(q) dq \sim W^{\zeta}, \quad (81)$$

which allows us to write the following scaling behavior

$$\chi_{\rho}(W, R) = R^{\zeta} f(W/R) = W^{\zeta} g(W/R). \quad (82)$$

Finally, it is possible to show that the re-scaled metastate-averaged probability distribution is Gaussian:¹⁰¹ $P_{\rho}(q/(W^{-(\zeta-D)/2}))$.

In Fig. 12, we present the behavior of the standard probability distribution of the overlap, $P(q)$, and the metastate one. The first point is that both probabilities are completely different. Moreover, for large values of W the Gaussian shape of $P_{\rho}(q)$ starts to be emerging.

The scaling of the metastate susceptibility allows to compute the ζ -exponent obtained, $\zeta = 2.3(3)$. This value compares very well with the

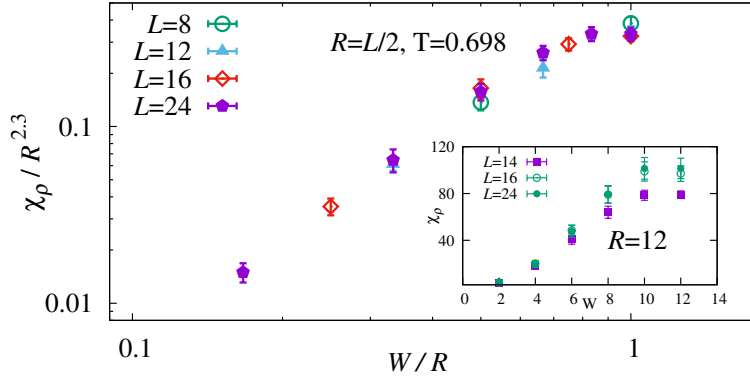


Fig. 13. Scaling behavior of the metastate susceptibility χ_ρ as a function of W/R for $R = L/2$ at $T \simeq 0.64T_c$. In the small panel we show the breakdown of the scaling behavior (asymptotic) which happens as $R/L > 3/4$.⁹⁹

replicon exponent $\zeta = 2.62(2)$, providing support for the Read conjecture regarding both exponents are the same. As a test of the computed value, we show in Fig. 13 a scaling plot of the re-scaled susceptibility, see Eq. (82).

Finally, we present in Fig. 14 the dependence of the Read ζ -exponent on the space dimension, marking the mean-field value (the horizontal value for $D \geq D_U = 6$), and the values obtained in numerical works.⁹⁹

Therefore, the numerical implementation of the metastate approach unveil a structure of the low temperature phase with a disperse metastate (i.e. $D > \zeta$). Only chaotic pairs and the RSB theory satisfy the property to have a dispersed metastate and not the droplets.

4.4. Phase transition at $h \neq 0$

Since the work of de Almeida and Thouless⁵⁶ forty years ago, a large amount of work has been devoted to understand the behavior of spin glasses in presence of a magnetic field (see Sec. 3.5). In particular during this long period of time a huge number of numerical simulations have been performed,^{4-6,120-136} though, a complete understanding of the model in a field is still lacking. One of the reasons is that strong finite size corrections are present in these systems which mask the infinite volume behavior.

As in the case of the $h = 0$ numerical simulations, we have initially based our analysis on the study of the behavior of the correlation length in units of the lattice size R_ξ . To do that, we need to compute a critical

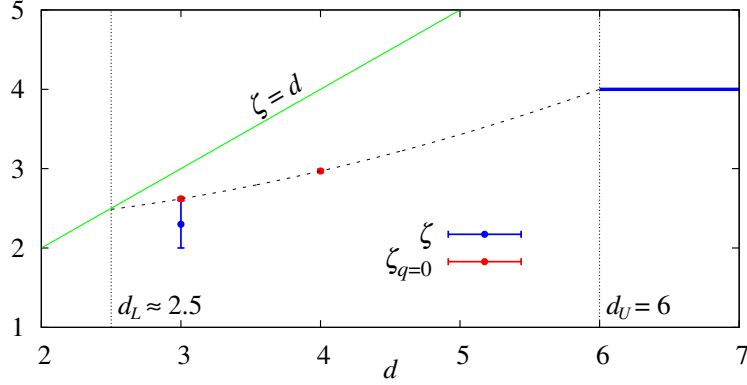


Fig. 14. The ζ -exponent against dimensionality $d \equiv D$.⁹⁹ In blue we have marked the known values (mean-field and $D = 3$ computed in Ref. [99]). In red we have marked the replicon exponent computed in numerical simulations at different dimensionalities (the Read conjecture is $\zeta = D - \theta(0)$). In green the droplet prediction for a non disperse metastate $D = \zeta$. Finally, we have drawn vertical lines at the lower and upper critical dimensions ($D_l \simeq 2.5$ and $D_u = 6$).⁹⁹

correlation function. In particular, in presence of a magnetic field, one can extract the critical behavior from two different correlation functions

$$G_1(\mathbf{r}) = \frac{1}{L^4} \sum_{\mathbf{x}} \overline{(\langle s_{\mathbf{x}} s_{\mathbf{x}+\mathbf{r}} \rangle - \langle s_{\mathbf{x}} \rangle \langle s_{\mathbf{x}+\mathbf{r}} \rangle)^2}, \quad (83)$$

$$G_2(\mathbf{r}) = \frac{1}{L^4} \sum_{\mathbf{x}} \overline{(\langle s_{\mathbf{x}} s_{\mathbf{x}+\mathbf{r}} \rangle^2 - \langle s_{\mathbf{x}} \rangle^2 \langle s_{\mathbf{x}+\mathbf{r}} \rangle^2)}. \quad (84)$$

Both correlation functions have the same critical behavior. The associated correlation lengths are computed in the usual way by calling Eq. (62).

This correlation length in units of the lattice size has worked pretty well in characterizing the phase transition at $h = 0$ (see Sec. 4.1). However, in presence of a magnetic field, it fails to identify a phase transition via the usual crossing point of the different curves computed with different lattice sizes, see the top panels of Fig. 15 and the left panels of Fig. 16. This lack of crossing on the ξ/L -curves has been interpreted in the past as a clear signal for a stable paramagnetic phase for all positive temperatures (i.e. there is no phase transition).

However, in some models based on random graphs, the phase transition has not been found numerically even in models where the phase transition has already been characterized analytically.^{137,138}

In order to analyze the origin of these strong finite size effects, which

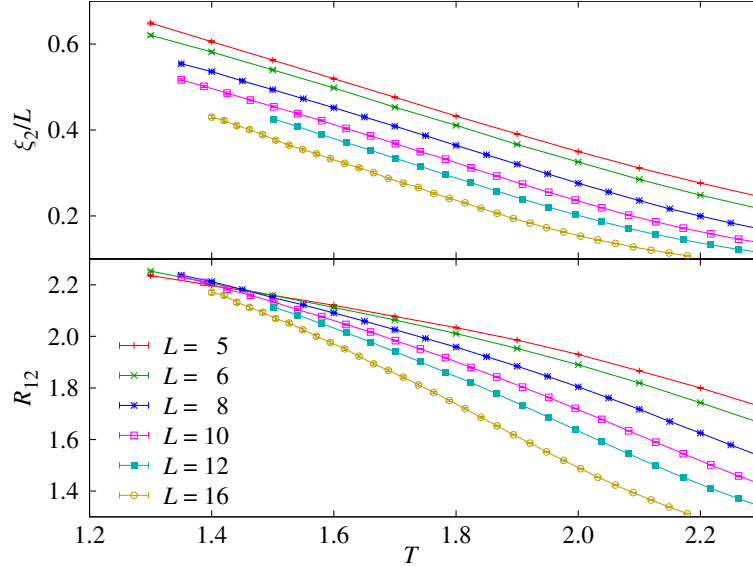


Fig. 15. In the top panel we show ξ_2/L for the simulated lattice sizes at $h = 0.15$. Notice the lack of crossing points of this cumulant. The absence of these crossing points has been interpreted as a clear signature of a paramagnetic phase in the whole region of positive temperatures. However, as explained in the main text, this behavior can be associated with the presence of the zero mode in the definition of the correlation length. In the bottom panel, we show the different curves for the R_{12} cumulant, which avoids the zero mode in its definition. This observable presents crossing points for the different lattices, therefore, it is possible to characterize a second order phase transition, including the critical temperature and exponents.¹³⁴

could spoil the crossing of the cumulants, we can compare the mean-field probability density function of the overlap, $P(q)$, with the one computed in a numerical simulation working on finite systems. In Fig. 17-top we show the numerical $P(q)$ for different values of a magnetic field, and in the bottom panel the mean-field prediction. Notice that the support of the analytical $P(q)$ is fully contained in the positive overlap axis and the same happens for the $P(q)$ in the droplet theory. Instead, the numerical $P(q)$ still shows large tails in the negative overlap region. These tails in the negative overlap region bias the correlation length, mainly via the zero mode used in its definition. Furthermore, the spin glass susceptibility, which is the Fourier transform of the correlation function computed a zero momentum, strongly suffers from the existence of these tails in $P(q)$. Another way to understand this phenomena is, following Refs. [136,139], realizing that the final results are dominated by atypical measurements. Focusing on typical

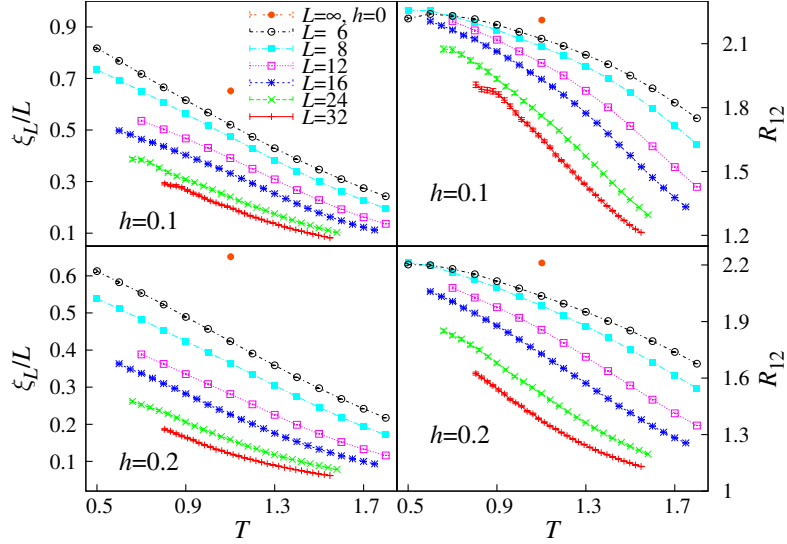


Fig. 16. We plot in the left panels ξ/L (and R_{12} in the right panels) as a function of the temperature for $h = 0.1$ and $h = 0.2$. As happens for $h = 0.15$, see Fig. 15, the R_{12} -curves cross but those of ξ/L ratio do not.¹³⁴

measurements will improve the final description of these systems.

Table 2. Summary of the critical exponents and the critical temperatures for three magnetic fields.¹³⁴

Parameters	$h = 0.3$	$h = 0.15$	$h = 0.075$
$T_c(h)$	0.906(40)[3]	1.229(30)[2]	1.50(7)
ν	1.46(7)[6]	—	—
η	-0.30(4)[1]	—	—

To avoid the strong effects induced by the zero mode we defined a new cumulant using the two smallest (and non-zero) momenta. The R_{12} has been used and defined in the section devoted to $h = 0$ (see Eq. (69)), but for the commodity of the reader we repeat here its definition particularizing in four dimensions

$$R_{12} = \frac{\tilde{G}(\mathbf{k}_1)}{\tilde{G}(\mathbf{k}_2)}, \quad (85)$$

where $\mathbf{k}_1 = (2\pi/L, 0, 0, 0)$ and $\mathbf{k}_2 = (2\pi/L, 2\pi/L, 0, 0)$ (plus permutations) are the two non-zero smallest momenta allowed by the periodic boundary conditions imposed at the system.¹³⁴

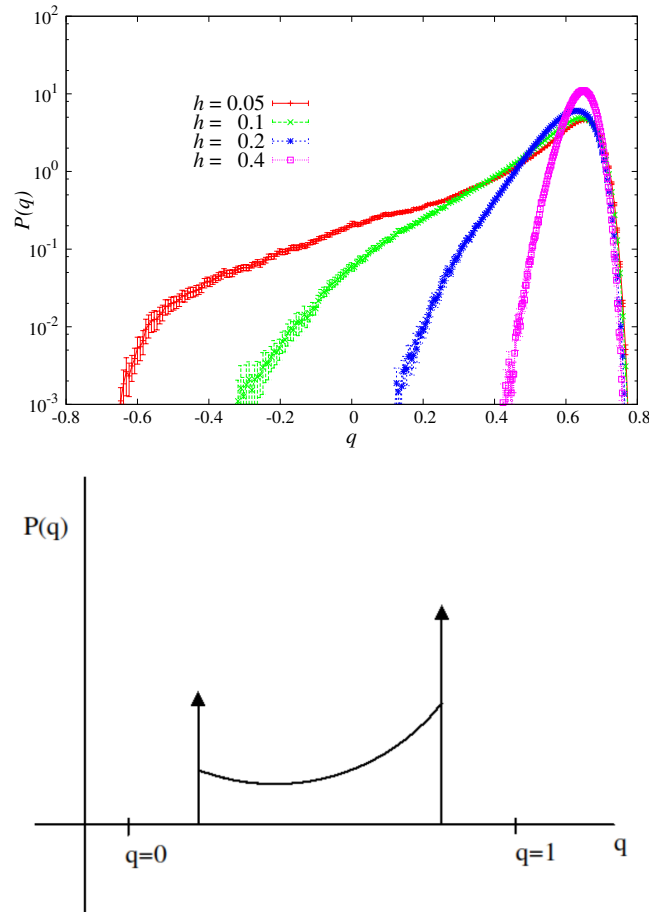


Fig. 17. $P(q)$ from numerical simulations (top) and RSB prediction (bottom) for the probability distribution of the overlap in the spin glass phase in presence of a magnetic field. The big arrows in the bottom panel represent delta functions. The RSB $P(q)$ function is different from zero only for positive overlaps.¹³⁴

Fig. 15-bottom shows that the cumulant R_{12} signals the phase transition. Its value at the critical point, as for other cumulants, is universal. Using these R_{12} crossing points it has been possible to characterize the phase transition in four dimension. Furthermore, it is possible to show that the critical exponents are independent of the strength of the magnetic field (taking into account corrections to scaling). In Table 2 we report the values computed for the critical exponents and the critical temperatures.

The analysis of the numerical data was performed working at constant coupling, see Sec. A.1 for a description of this method.

We can analyze the scaling behavior of these critical temperature performing a test of the Fisher-Sompolinsky relation:⁶¹

$$h^2(T_c) \simeq A|T_c(h) - T_c(0)|^{\beta^{(0)} + \gamma^{(0)}}, \quad (86)$$

where $T_c(h)$ is the critical temperature in a field, and the symbols with a zero as superscript refer to the critical properties of the model in zero magnetic field: critical temperature and exponents.

In the inset of Fig. 18 we report this analysis finding a very good agreement between the numerical results (for the computed critical temperatures) and the previous relation. In addition, the fit has only one free parameter.

However, using this methodology, no traces of a phase transition in the three dimensional model in a field has been found. The simplest explanation is that the lower critical dimension of the model in a magnetic field ($3 < D_l < 4$) is different of that in $h = 0$ ($D_l = 2.5$), as happens in the random field Ising model case (the lower critical dimension in $h = 0$ is one and in presence of a random magnetic field is two).

5. Conclusions

We have presented an overview of different analytical approaches to finite dimensional Ising spin glasses. The analytical approach based on field theory is still incomplete both for $h = 0$ and $h \neq 0$. In presence of a magnetic field, recent analytical work points out to a complicated structure of the critical behavior below the upper critical dimension.

Moreover, we have presented numerical evidence for existence of the spin glass phase in absence of a magnetic field. The properties of this low temperature phase fit very well in the framework of the RSB theory. Nextly, we have studied in detailed the replicon propagator and we have shown how a disperse metastate has been found. The situation in presence of a magnetic field is not clear. In particular, there is no evidence of a phase transition in three dimensions, though in four dimensions it has been found.

Acknowledgments

This work was partially supported by Ministerio de Economía y Competitividad (Spain) through Grant No. FIS2016-76359-P, by Junta de Ex-

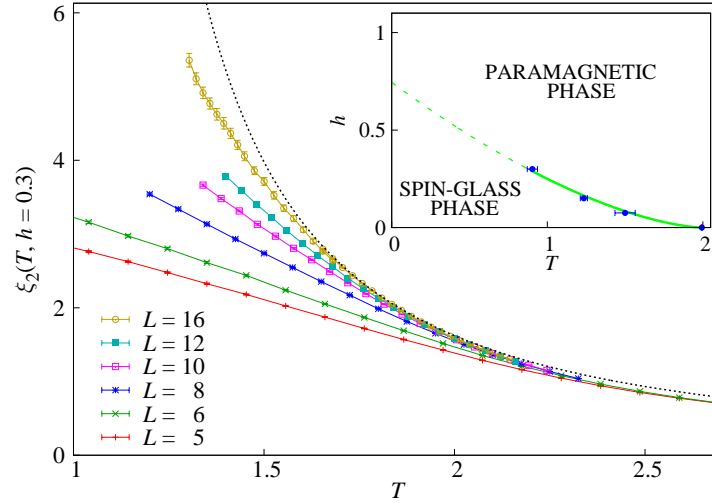


Fig. 18. In the inset we plot the Fisher-Sompolinsky relation for a four-dimensional spin glass with binary couplings: $h^2(T_c) \simeq A|T_c(h) - T_c(0)|^{\beta^{(0)} + \gamma^{(0)}}$. Notice that there is only one free parameter in the fit. In the main plot, we present behavior of the correlation length for different lattice sizes with the infinite volume extrapolation at $h = 0.3$ (continuous dotted line).¹³⁴

tremadura (Spain) through Grants No. GRU18079 and IB16013 (partially funded by FEDER).

I have enjoyed interesting and fruitful discussions on spin glasses and numerical simulations with M. Baity-Jesi, A. Billoire, A. Cruz, L.A. Fernandez, A. Gordillo-Guerrero, D. Iñiguez, R. Kenna, A. Lasanta, L. Leuzzi, A. Maiorano, E. Marinari, V. Martin-Mayor, J. Monforte, A. Muñoz-Sdupe, D. Navarro, G. Parisi, S. Perez-Gaviro, F. Ricci-Tersenghi, B. Seoane, A. Tarancon, R. Tripicciono and D. Yllanes.

I warmly thank Yu. Holovatch and E. Ruiz Espejo for a careful reading of the manuscript.

Finally, I would like to thank M. Dudka and Yu. Holovatch for inviting me to present these results in the 2019 Lviv Ising Lectures.

A.1. Characterization of a phase transition: Quotient and fixed coupling methods

Let us consider a quantity $O(\beta, L)$ which scales in the thermodynamic limit as $\xi^{x_O/\nu}$. We can study the behavior of this observable by computing it at L and $2L$, $\mathcal{Q}_O = O_{2L}/O_L$, at the crossing point $\beta_{\text{cross}}(L, 2L)$ of R_ξ or U_4 . In the case of a dimensionless observable the exponent $x_O = 0$. We will denote as g all the dimensionless quantities.³⁶

Hence, one gets

$$\mathcal{Q}_O^{\text{cross}} = 2^{x_O/\nu} + \mathcal{O}(L^{-\omega}), \quad (\text{A.1})$$

or

$$g^{\text{cross}} = g^* + \mathcal{O}(L^{-\omega}), \quad (\text{A.2})$$

where x_O/ν , g^* and the correction-to-scaling exponent ω are universal quantities. Examples of dimensionless quantities are R_ξ and the cumulants (e.g. U_4 and U_{22}). We could also consider dimensionful observables as the susceptibility ($x_\chi = \nu(2 - \eta)$) and the β -derivatives of R_ξ and U_4 ($x = 1$ for both).

The behavior of the crossing points of the inverse temperature ($\beta_{\text{cross}}(L, 2L)$) are given by

$$\beta_{\text{cross}}(L, 2L) = \beta_c + A_{\beta_c, g} L^{-\omega-1/\nu} + \dots, \quad (\text{A.3})$$

where in our case $g = R_\xi$ or U_4 .

In order to study the leading correction-to-scaling exponent we can build the quotient of a given dimensionless quantity g

$$\mathcal{Q}_g = g_{2L}/g_L$$

at $\beta_{\text{cross}}(L, 2L)$. This quotient behaves as

$$\mathcal{Q}_g^{\text{cross}}(L) = 1 + A_g L^{-\omega} + B_g L^{-2\omega} + \dots \quad (\text{A.4})$$

In the fixed coupling method the analysis is slightly different. For instance we have a fixed value of a dimensionless observable $g = g_f$ near the universal one (for example a given value of R_ξ) and we compute the value of $\beta(L)$ at which

$$g_f = g(\beta(g_f, L), L). \quad (\text{A.5})$$

At this value of the inverse temperature we can study scaling of the derivatives of different observables (e.g. susceptibility, derivatives of R_ξ and Binder cumulant, etc.) which allows to extract the critical exponents via

$$O(\beta(g_f, L), L) = A(g_f) L^{x_O/\nu} \left(1 + \mathcal{O}\left(\frac{1}{L^\omega}\right) \right). \quad (\text{A.6})$$

A.2. The Janus supercomputers

Most of the numerical simulations presented in this chapter were obtained using the Janus I and II supercomputers. These computers were built to take advantage of the powerful integer arithmetic and a high number of processor units of the FPGA (Fast Programmable Devices). They were designed and used by a scientific collaboration composed by researchers of two Italian Universities, Ferrara and Roma I “La Sapienza” and three Spanish ones: Complutense de Madrid, Zaragoza and Extremadura.

The physics obtained with the help of the Janus supercomputers^{28,29,80,81,109,134–136,140–144} has covered a wide variety of spin models, mainly Ising spin glass but also Potts glass models. These discrete models allow the supercomputers to achieve their maximum performance.



Fig. A.1. External view of the Janus I supercomputer during its presentation in Italy.

The Janus I computer, see Fig. A.1, entered in production mode in 2008.^{145–148} Its most important features are:

- It is composed by 16 boards of 16 FPGAs each (Virtex 4).
- For Ising models, Janus I is equivalent to 10000 PC.
- High degree of parallelization inside the boards.

- Janus allows us to simulate in the 0.1 s time region. Usually, experimental times range from 1 s to 3000 s and previous numerical simulations simulated the 10^{-5} s region (SSUE).

The next generation of Janus computer, the Janus II one, was built in 2015 and its principal characteristic are:¹⁴⁹

- Janus II is 5 times most powerful than Janus.
- It is still a dedicated computer optimized to simulate a wide variety of spin models.
- It presents a more flexible topology.
- It is formed by 16 boards of 16 FPGAs each (one IOP and PC integrated on each board) (Virtex 7).
- Janus II allows to simulate in the 1 second time region.

References

1. J. A. Mydosh, *Spin Glasses: an Experimental Introduction*. Taylor and Francis, London (1993).
2. G. Kotliar, P. W. Anderson, and D. L. Stein, One-dimensional spin-glass model with long-range random interactions, *Phys. Rev. B.* **27**, 602 (1983). doi: 10.1103/PhysRevB.27.602.
3. L. Leuzzi, Critical behaviour and ultrametricity of Ising spin-glass with long-range interactions, *Journal of Physics A: Mathematical and General.* **32** (8), 1417–1426 (jan, 1999). doi: 10.1088/0305-4470/32/8/010. URL <https://doi.org/10.1088/0305-4470/32/8/010>.
4. L. Leuzzi, G. Parisi, F. Ricci-Tersenghi, and J. J. Ruiz-Lorenzo, Ising spin-glass transition in a magnetic field outside the limit of validity of mean-field theory, *Phys. Rev. Lett.* **103**, 267201 (2009). doi: 10.1103/PhysRevLett.103.267201.
5. L. Leuzzi, G. Parisi, F. Ricci-Tersenghi, and J. Ruiz-Lorenzo, Bond diluted Levy spin-glass model and a new finite-size scaling method to determine a phase transition, *Philosophical Magazine.* **91**(13-15), 1917–1925 (2011). doi: 10.1080/14786435.2010.534741. URL <https://doi.org/10.1080/14786435.2010.534741>.
6. D. Larson, H. G. Katzgraber, M. A. Moore, and A. P. Young, Spin glasses in a field: Three and four dimensions as seen from one space dimension, *Phys. Rev. B.* **87**, 024414 (2013). doi: 10.1103/PhysRevB.87.024414.
7. L. Leuzzi, G. Parisi, F. Ricci-Tersenghi, and J. J. Ruiz-Lorenzo, Infinite volume extrapolation in the one-dimensional bond diluted Levy spin-glass model near its lower critical dimension, *Phys. Rev. B.* **91**, 064202 (Feb, 2015). doi: 10.1103/PhysRevB.91.064202. URL <https://link.aps.org/doi/10.1103/PhysRevB.91.064202>.

8. M. Dilucca, L. Leuzzi, G. Parisi, F. Ricci-Tersenghi, and J. J. Ruiz-Lorenzo, Spin glasses in a field show a phase transition varying the distance among real replicas (and how to exploit it to find the critical line in a field), *Entropy*. **22(2)**, 250 (2020).
9. H. Katzgraber and A. P. Young, Monte Carlo studies of the one-dimensional ising spin glass with power-law interactions, *Phys. Rev. B*. **67**, 134410 (2003). doi: 10.1103/PhysRevB.67.134410.
10. H. G. Katzgraber and A. P. Young, Probing the Almeida-Thouless line away from the mean-field model, *Phys. Rev. B*. **72**, 184416 (Nov, 2005). doi: 10.1103/PhysRevB.72.184416. URL <https://link.aps.org/doi/10.1103/PhysRevB.72.184416>.
11. H. G. Katzgraber, T. Jörg, F. Krzakala, and A. K. Hartmann, Ultrametric probe of the spin-glass state in a field, *Phys. Rev. B*. **86**, 184405 (Nov, 2012). doi: 10.1103/PhysRevB.86.184405. URL <https://link.aps.org/doi/10.1103/PhysRevB.86.184405>.
12. H. G. Katzgraber, D. Larson, and A. P. Young, Study of the de Almeida–Thouless line using power-law diluted one-dimensional Ising spin glasses, *Phys. Rev. Lett.* **102**, 177205 (Apr, 2009). doi: 10.1103/PhysRevLett.102.177205. URL <https://link.aps.org/doi/10.1103/PhysRevLett.102.177205>.
13. H. G. Katzgraber and A. K. Hartmann, Ultrametricity and clustering of states in spin glasses: A one-dimensional view, *Phys. Rev. Lett.* **102**, 037207 (Jan, 2009). doi: 10.1103/PhysRevLett.102.037207. URL <https://link.aps.org/doi/10.1103/PhysRevLett.102.037207>.
14. T. Aspelmeier, H. G. Katzgraber, D. Larson, M. A. Moore, M. Wittmann, and J. Yeo, Finite-size critical scaling in Ising spin glasses in the mean-field regime, *Phys. Rev. E*. **93**, 032123 (Mar, 2016). doi: 10.1103/PhysRevE.93.032123. URL <https://link.aps.org/doi/10.1103/PhysRevE.93.032123>.
15. K. Binder and A. P. Young, Spin glasses: Experimental facts, theoretical concepts, and open questions, *Rev. Mod. Phys.* **58**, 801–976 (Oct, 1986). doi: 10.1103/RevModPhys.58.801. URL <http://link.aps.org/doi/10.1103/RevModPhys.58.801>.
16. A. P. Young, *Spin Glasses and Random Fields*. World Scientific, Singapore (1998). doi: 10.1142/3517.
17. C. de Dominicis and I. Giardinà, *Random Fields and Spin Glasses: a field theory approach*. Cambridge University Press, Cambridge, England (2006).
18. K. H. Fischer and J. A. Hertz, *Spin Glasses*. Cambridge University Press (1993).
19. M. Ruderman and C. Kittel, Indirect exchange coupling of nuclear magnetic moments by conduction electrons, *Phys. Rev.* **96**, 99 (1954).
20. T. Kasuya, A theory of metallic ferro- and antiferromagnetism on zener’s model, *Prog. Theor. Phys.* **16**, 45 (1956).
21. K. Yosida, Magnetic properties of Cu-Mn alloys, *Phys. Rev.* **106**, 893–898 (Jun, 1957). doi: 10.1103/PhysRev.106.893. URL <http://link.aps.org/doi/10.1103/PhysRev.106.893>.
22. S. Guchhait and R. Orbach, Direct dynamical evidence for the spin glass

- lower critical dimension $2 < d < 3$, *Phys. Rev. Lett.* **112**, 126401 (Mar, 2014). doi: 10.1103/PhysRevLett.112.126401. URL <http://link.aps.org/doi/10.1103/PhysRevLett.112.126401>.
23. S. Guchhait, G. G. Kenning, R. L. Orbach, and G. F. Rodriguez, Spin glass dynamics at the mesoscale, *Phys. Rev. B.* **91**, 014434 (Jan, 2015). doi: 10.1103/PhysRevB.91.014434. URL <http://link.aps.org/doi/10.1103/PhysRevB.91.014434>.
 24. S. Guchhait and R. L. Orbach, Temperature chaos in a Ge:Mn thin-film spin glass, *Phys. Rev. B.* **92**, 214418 (Dec, 2015). doi: 10.1103/PhysRevB.92.214418. URL <http://link.aps.org/doi/10.1103/PhysRevB.92.214418>.
 25. S. Guchhait and R. L. Orbach, Magnetic field dependence of spin glass free energy barriers, *Phys. Rev. Lett.* **118**, 157203 (Apr, 2017). doi: 10.1103/PhysRevLett.118.157203. URL <https://link.aps.org/doi/10.1103/PhysRevLett.118.157203>.
 26. Y. G. Joh, R. Orbach, G. G. Wood, J. Hammann, and E. Vincent, Extraction of the spin glass correlation length, *Phys. Rev. Lett.* **82**, 438–441 (Jan, 1999). doi: 10.1103/PhysRevLett.82.438. URL <http://link.aps.org/doi/10.1103/PhysRevLett.82.438>.
 27. Q. Zhai, D. C. Harrison, D. Tennant, E. D. Dalhberg, G. G. Kenning, and R. L. Orbach, Glassy dynamics in CuMn thin-film multilayers, *Phys. Rev. B.* **95**, 054304 (Feb, 2017). doi: 10.1103/PhysRevB.95.054304. URL <https://link.aps.org/doi/10.1103/PhysRevB.95.054304>.
 28. M. Baity-Jesi, E. Calore, A. Cruz, L. A. Fernandez, J. M. Gil-Narvion, A. Gordillo-Guerrero, D. Iñiguez, A. Maiorano, E. Marinari, V. Martin-Mayor, J. Monforte-Garcia, A. Muñoz Sudupe, D. Navarro, G. Parisi, S. Perez-Gaviro, F. Ricci-Tersenghi, J. J. Ruiz-Lorenzo, S. F. Schifano, B. Seoane, A. Tarancon, R. Tripiccion, and D. Yllanes, Matching microscopic and macroscopic responses in glasses, *Phys. Rev. Lett.* **118**, 157202 (Apr, 2017). doi: 10.1103/PhysRevLett.118.157202. URL <https://link.aps.org/doi/10.1103/PhysRevLett.118.157202>.
 29. M. Baity-Jesi, E. Calore, A. Cruz, L. A. Fernandez, J. M. Gil-Narvion, A. Gordillo-Guerrero, D. Iñiguez, A. Maiorano, E. Marinari, V. Martin-Mayor, J. Moreno-Gordo, A. Muñoz Sudupe, D. Navarro, G. Parisi, S. Perez-Gaviro, F. Ricci-Tersenghi, J. J. Ruiz-Lorenzo, S. F. Schifano, B. Seoane, A. Tarancon, R. Tripiccion, and D. Yllanes, Aging rate of spin glasses from simulations matches experiments, *Phys. Rev. Lett.* **120**, 267203 (Jun, 2018). doi: 10.1103/PhysRevLett.120.267203. URL <https://link.aps.org/doi/10.1103/PhysRevLett.120.267203>.
 30. L. A. Fernandez, E. Marinari, V. Martin-Mayor, I. Paga, and J. J. Ruiz-Lorenzo, Dimensional crossover in the aging dynamics of spin glasses in a film geometry, *Phys. Rev. B.* **100**, 184412 (Nov, 2019). doi: 10.1103/PhysRevB.100.184412. URL <https://link.aps.org/doi/10.1103/PhysRevB.100.184412>.
 31. S. F. Edwards and P. W. Anderson, Theory of spin glasses, *Journal of Physics F: Metal Physics.* **5**, 965 (1975). doi: 10.1088/0305-4608/5/5/017. URL <http://stacks.iop.org/0305-4608/5/i=5/a=017>.

32. M. Mézard, G. Parisi, and M. Virasoro, *Spin-Glass Theory and Beyond*. World Scientific, Singapore (1987). doi: 10.1142/0271.
33. S. Kirkpatrick and D. Sherrington, Infinite-ranged models of spin-glasses, *Phys. Rev. B*, **17**, 4384–4403 (Jun, 1978). doi: 10.1103/PhysRevB.17.4384. URL <http://link.aps.org/doi/10.1103/PhysRevB.17.4384>.
34. V. Dotsenko, *Introduction to the Replica Theory of Disordered Statistical Systems*. Cambridge University Press, Cambridge, England (2001).
35. J. Cardy, *Scaling and Renormalization in Statistical Physics*. vol. 5, *Lecture notes in physics*, Cambridge University Press, Cambridge (1996). ISBN 0521499593.
36. D. J. Amit and V. Martín-Mayor, *Field Theory, the Renormalization Group and Critical Phenomena*, third edn. World Scientific, Singapore (2005). doi: 10.1142/9789812775313_bmatter. URL <http://www.worldscientific.com/worldscibooks/10.1142/5715>.
37. G. Parisi, *Statistical Field Theory*. Addison-Wesley (1988).
38. C. Itzykson and J. M. Drouffe, *Statistical Field Theory*. Cambridge University Press (1989).
39. G. Parisi, Infinite number of order parameters for spin-glasses, *Phys. Rev. Lett.* **43**, 1754–1756 (Dec, 1979). doi: 10.1103/PhysRevLett.43.1754. URL <http://link.aps.org/doi/10.1103/PhysRevLett.43.1754>.
40. G. Parisi, Toward a mean-field theory for spin glasses, *Phys. Lett.* **73A**, 203 (1979). doi: 10.1016/0375-9601(79)90708-4.
41. G. Parisi, The order parameter for spin glasses: a function on the interval 0-1, *J. Phys. A: Math. Gen.* **13**, 1101 (1980). doi: 10.1088/0305-4470/13/3/042.
42. G. Parisi, A sequence of approximated solutions to the S-K model for spin glasses, *J. Phys. A: Math. Gen.* **13**, L115–L121 (1980). ISSN 0305-4470. doi: 10.1088/0305-4470/13/4/009.
43. G. Parisi, Magnetic properties of spin glasses in a new mean-field theory, *Journal of Physics A: Mathematical and General*. **13**(5), 1887 (1980). doi: 10.1088/0305-4470/13/5/047. URL <http://stacks.iop.org/0305-4470/13/i=5/a=047>.
44. G. Parisi, Order parameter for spin glasses, *Phys. Rev. Lett.* **50**, 1946 (1983). doi: 10.1103/PhysRevLett.50.1946. URL <http://journals.aps.org/prl/abstract/10.1103/PhysRevLett.50.1946>.
45. J. Monforte. *Rugged Free-Energy Landscapes in Disordered Spin Systems*. PhD thesis, Universidad de Zaragoza (2013). URL <http://zaguan.unizar.es/record/11743/files/TESIS-2013-077.pdf>.
46. M. Mézard, G. Parisi, N. Sourlas, G. Toulouse, and M. Virasoro, Nature of the spin-glass phase, *Phys. Rev. Lett.* **52**, 1156 (1984). doi: 10.1103/PhysRevLett.52.1156.
47. M. Mézard, G. Parisi, N. Sourlas, G. Toulouse, and M. Virasoro, Replica symmetry breaking and the nature of the spin glass phase, *J. Phys. France*. **45**, 843–854 (1984). doi: 10.1051/jphys:01984004505084300.
48. M. Mézard and M. Virasoro, On the microstructure of ultrametricity, *J. Physique*. **46**, 1293–1307 (1985). doi: 10.1051/jphys:019850046080129300.

49. M. Mézard, G. Parisi, and M. Virasoro, Random free energies in spin glasses, *J. Physique Lett.* **46**, 217–222 (1985). doi: 10.1051/jphyslet:01985004606021700.
50. M. Mézard, G. Parisi, and M. Virasoro, Sk model: The replica solution without replicas, *Europhys. Lett.* **1**, 77 (1986). doi: 10.1209/0295-5075/1/2/006.
51. E. Marinari, G. Parisi, F. Ricci-Tersenghi, J. J. Ruiz-Lorenzo, and F. Zuliani, Replica symmetry breaking in short-range spin glasses: Theoretical foundations and numerical evidences, *J. Stat. Phys.* **98**, 973 (2000). doi: 10.1023/A:1018607809852.
52. F. Guerra, Broken replica symmetry bounds in the mean-field spin glass model, *Comm. Math. Phys.* **233**, 1–12 (2003). doi: 10.1007/s00220-002-0773-5.
53. M. Talagrand, *Mean Field Models for Spin Glasses*. Springer-Verlag, Berlin (2011).
54. D. Panchenko, *The Sherrington-Kirkpatrick Model*. Springer-Verlag, Berlin (2013).
55. R. Rammal, G. Toulouse, and M. A. Virasoro, Ultrametricity for physicists, *Rev. Mod. Phys.* **58**, 765–788 (Jul, 1986). doi: 10.1103/RevModPhys.58.765. URL <http://link.aps.org/doi/10.1103/RevModPhys.58.765>.
56. J. R. L. de Almeida and D. J. Thouless, Stability of the Sherrington-Kirkpatrick solution of a spin glass model, *J. Phys. A: Math. Gen.* **11**, 983 (1978). doi: 10.1088/0305-4470/11/5/028. URL <http://stacks.iop.org/0305-4470/11/i=5/a=028>.
57. K. G. Wilson and J. Kogut, The renormalization group and the ϵ -expansion, *Physics Reports.* **12**(2), 75 – 199 (1974). ISSN 0370-1573. doi: 10.1016/0370-1573(74)90023-4. URL <http://www.sciencedirect.com/science/article/pii/0370157374900234>.
58. K. G. Wilson, The renormalization group: Critical phenomena and the Kondo problem, *Rev. Mod. Phys.* **47**, 773–840 (Oct, 1975). doi: 10.1103/RevModPhys.47.773. URL <http://link.aps.org/doi/10.1103/RevModPhys.47.773>.
59. A. J. Bray and M. A. Moore. Scaling theory of the ordered phase of spin glasses. In eds. J. L. van Hemmen and I. Morgenstern, *Heidelberg Colloquium on Glassy Dynamics*, number 275 in Lecture Notes in Physics. Springer, Berlin (1987).
60. A. J. Bray and M. A. Moore, Chaotic nature of the spin-glass phase, *Phys. Rev. Lett.* **58**, 57–60 (Jan, 1987). doi: 10.1103/PhysRevLett.58.57. URL <https://link.aps.org/doi/10.1103/PhysRevLett.58.57>.
61. D. S. Fisher and H. Sompolinsky, Scaling in spin-glasses, *Phys. Rev. Lett.* **54**, 1063 (1985). doi: 10.1103/PhysRevLett.54.1063.
62. D. S. Fisher and D. A. Huse, Ordered phase of short-range Ising spin-glasses, *Phys. Rev. Lett.* **56**, 1601 (Apr, 1986). doi: 10.1103/PhysRevLett.56.1601. URL <http://link.aps.org/doi/10.1103/PhysRevLett.56.1601>.
63. D. S. Fisher and D. A. Huse, Nonequilibrium dynamics of spin glasses, *Phys. Rev. B.* **38**, 373–385 (Jul, 1988). doi: 10.1103/PhysRevB.38.373. URL

- <https://link.aps.org/doi/10.1103/PhysRevB.38.373>.
64. D. S. Fisher and D. A. Huse, Equilibrium behavior of the spin-glass ordered phase, *Phys. Rev. B.* **38**, 386 (1988). doi: 10.1103/PhysRevB.38.386.
 65. A. B. Harris, T. C. Lubensky, and J.-H. Chen, Critical properties of spin-glasses, *Phys. Rev. Lett.* **36**, 415–418 (Feb, 1976). doi: 10.1103/PhysRevLett.36.415. URL <http://link.aps.org/doi/10.1103/PhysRevLett.36.415>.
 66. O. F. de Alcantara Bonfim, J. E. Kirkham, and A. J. McKane, Critical exponents for the percolation problem and the yang-lee edge singularity, *Journal of Physics A: Mathematical and General.* **14**(9), 2391–2413 (sep, 1981). doi: 10.1088/0305-4470/14/9/034. URL <https://doi.org/10.1088/0305-4470/14/9/034>.
 67. J. E. Green, ϵ -expansion for the critical exponents of a vector spin glass, *Journal of Physics A: Mathematical and General.* **18**(1), L43–L47 (jan, 1985). doi: 10.1088/0305-4470/18/1/008. URL <https://doi.org/10.1088/0305-4470/18/1/008>.
 68. J. J. Ruiz-Lorenzo, Logarithmic corrections for spin glasses, percolation and lee-yang singularities in six dimensions, *J. Phys. A: Math. Gen.* **31**, 8773 (1998).
 69. R. Kenna, D. A. Johnston, and W. Janke, Scaling relations for logarithmic corrections, *Phys. Rev. Lett.* **96**, 115701 (Mar, 2006). doi: 10.1103/PhysRevLett.96.115701. URL <https://link.aps.org/doi/10.1103/PhysRevLett.96.115701>.
 70. R. Kenna, D. A. Johnston, and W. Janke, Self-consistent scaling theory for logarithmic-correction exponents, *Phys. Rev. Lett.* **97**, 155702 (Oct, 2006). doi: 10.1103/PhysRevLett.97.155702. URL <https://link.aps.org/doi/10.1103/PhysRevLett.97.155702>.
 71. R. Kenna. Universal scaling relations for logarithmic-correction exponents. In ed. Yu. Holovatch, *Order, Disorder and Criticality, vol. 3, pp. 1-46*. World Scientific, Singapore (2013).
 72. J. J. Ruiz-Lorenzo, Revisiting (logarithmic) scaling relations using renormalization group, *Condens. Matter Phys.* **20**, 13601 (2017).
 73. S. Franz, G. Parisi, and M. A. Virasoro, The replica method on and off equilibrium, *J. Phys. I (France).* **2**, 1869 (1992). doi: 10.1051/jp1:1992115.
 74. S. Boettcher, Stiffness of the Edwards-Anderson model in all dimensions, *Phys. Rev. Lett.* **95**, 197205 (Nov, 2005). doi: 10.1103/PhysRevLett.95.197205. URL <http://link.aps.org/doi/10.1103/PhysRevLett.95.197205>.
 75. A. Maiorano and G. Parisi, Support for the value 5/2 for the spin glass lower critical dimension at zero magnetic field, *Proceedings of the National Academy of Sciences.* **115**(20), 5129–5134 (2018). ISSN 0027-8424. doi: 10.1073/pnas.1720832115. URL <https://www.pnas.org/content/115/20/5129>.
 76. C. de Dominicis, I. Kondor, and T. Temesvári, Ising spin glass: recent progress in the field theory approach, *Int. J. Mod. Phys. B.* **7**, 986 (1993). doi: 10.1142/S0217979293002134.

77. C. de Dominicis, I. Kondor, and T. Temesvári. Beyond the Sherrington-Kirkpatrick model. In ed. A. P. Young, *Spin Glasses and Random Fields*. World Scientific, Singapore (1998).
78. D. Iñiguez, G. Parisi, and J. J. Ruiz-Lorenzo, Simulation of 3d Ising spin glass model using three replicas: study of binder cumulants, *J. Phys. A: Math. and Gen.* **29**, 4337 (1996). doi: 10.1088/0305-4470/29/15/009.
79. G. Parisi and F. Ricci-Tersenghi, On the origin of ultrametricity, *J. Phys. A: Math. Gen.* **33**, 113 (2000). doi: 10.1088/0305-4470/33/1/307.
80. F. Belletti, A. Cruz, L. A. Fernandez, A. Gordillo-Guerrero, M. Guidetti, A. Maiorano, F. Mantovani, E. Marinari, V. Martín-Mayor, J. Monforte, A. Muñoz Sudupe, D. Navarro, G. Parisi, S. Perez-Gaviro, J. J. Ruiz-Lorenzo, S. F. Schifano, D. Sciretti, A. Tarancon, R. Tripiccion, and D. Yllanes, An in-depth look at the microscopic dynamics of Ising spin glasses at fixed temperature, *J. Stat. Phys.* **135**, 1121 (2009). doi: 10.1007/s10955-009-9727-z.
81. R. Alvarez Baños, A. Cruz, L. A. Fernandez, J. M. Gil-Narvion, A. Gordillo-Guerrero, M. Guidetti, A. Maiorano, F. Mantovani, E. Marinari, V. Martín-Mayor, J. Monforte-Garcia, A. Muñoz Sudupe, D. Navarro, G. Parisi, S. Perez-Gaviro, J. J. Ruiz-Lorenzo, S. F. Schifano, B. Seoane, A. Tarancon, R. Tripiccion, and D. Yllanes, Nature of the spin-glass phase at experimental length scales, *J. Stat. Mech.* **2010**, P06026 (2010). doi: 10.1088/1742-5468/2010/06/P06026.
82. F. Guerra, About the overlap distribution in mean-field spin glass models, *Int. J. Mod. Phys. B.* **10**, 1675 (1996).
83. S. Ghirlanda and F. Guerra, General properties of overlap probability distributions in disordered spin systems. towards Parisi ultrametricity, *J. Phys. A: Math. Gen.* **31**, 9149 (1998). doi: 10.1088/0305-4470/31/46/006.
84. P. Contucci, C. Giardinà, C. Giberti, G. Parisi, and C. Vernia, Ultrametricity in the Edwards-Anderson model, *Phys. Rev. Lett.* **99**, 057206 (2007). doi: 10.1103/PhysRevLett.99.057206.
85. G. Parisi, F. Ricci-Tersenghi, and J. J. Ruiz-Lorenzo, Generalized off-equilibrium fluctuation-dissipation relations in random Ising systems, *Eur. Phys. J.* **11**, 317–325 (1999). doi: 10.1007/s100510050942.
86. A. J. Bray and M. A. Moore, Disappearance of the de Almeida-Thouless line in six dimensions, *Phys. Rev. B.* **83**, 224408 (2011). doi: 10.1103/PhysRevB.83.224408.
87. A. J. Bray and S. A. Roberts, Renormalisation-group approach to the spin glass transition in finite magnetic fields, *J. Phys. C: Solid St. Phys.* **13**, 5405 (1980). doi: 10.1088/0022-3719/13/29/019.
88. P. Charbonneau and S. Yaida, Nontrivial critical fixed point for replica-symmetry-breaking transitions, *Phys. Rev. Lett.* **118**, 215701 (May, 2017). doi: 10.1103/PhysRevLett.118.215701. URL <https://link.aps.org/doi/10.1103/PhysRevLett.118.215701>.
89. B. Delamotte. Introduction to the non-perturbative renormalization group. In ed. Yu. Holovatch, *Order, Disorder and Criticality, vol. 2, pp. 1–77*. World Scientific, Singapore (2007).

90. I. R. Pimentel, T. Temesvári, and C. De Dominicis, Spin-glass transition in a magnetic field: A renormalization group study, *Phys. Rev. B.* **65**, 224420 (Jun, 2002). doi: 10.1103/PhysRevB.65.224420. URL <https://link.aps.org/doi/10.1103/PhysRevB.65.224420>.
91. T. Temesvári, Almeida-Thouless transition below six dimensions, *Phys. Rev. B.* **78**, 220401 (2008).
92. G. Parisi and T. Temesvári, Replica symmetry breaking in and around six dimensions, *Nucl. Phys. B.* **858**, 293 (2012).
93. J. Höller and N. Read, One-step replica-symmetry-breaking phase below the de Almeida-Thouless line in low-dimensional spin glasses, *arXiv e-prints*. art. arXiv:1909.03284 (2019).
94. D. Ruelle, *Statistical Mechanics*. Benjamin (1969).
95. G. Parisi, *Field Theory, Disorder and Simulations*. World Scientific (1994).
96. C. M. Newman and D. L. Stein, Multiple states and thermodynamic limits in short-ranged Ising spin-glass models, *Phys. Rev. B.* **46**, 973–982 (Jul, 1992). doi: 10.1103/PhysRevB.46.973.
97. C. M. Newman and D. L. Stein, Spatial inhomogeneity and thermodynamic chaos, *Phys. Rev. Lett.* **76**, 4821–4824 (Jun, 1996). doi: 10.1103/PhysRevLett.76.4821.
98. C. M. Newman and D. L. Stein, Simplicity of state and overlap structure in finite-volume realistic spin glasses, *Phys. Rev. E.* **57**, 1356–1366 (Feb, 1998). doi: 10.1103/PhysRevE.57.1356. URL <http://link.aps.org/doi/10.1103/PhysRevE.57.1356>.
99. A. Billoire, L. A. Fernandez, A. Maiorano, E. Marinari, V. Martin-Mayor, J. Moreno-Gordo, G. Parisi, F. Ricci-Tersenghi, and J. J. Ruiz-Lorenzo, Numerical construction of the Aizenman-Wehr metastate, *Phys. Rev. Lett.* **119**, 037203 (Jul, 2017). doi: 10.1103/PhysRevLett.119.037203. URL <https://link.aps.org/doi/10.1103/PhysRevLett.119.037203>.
100. M. Aizenman and J. Wehr, Rounding effects of quenched randomness on first-order phase transitions, *Communications in Mathematical Physics.* **130** (3), 489–528 (1990). ISSN 0010-3616. doi: 10.1007/BF02096933. URL <http://dx.doi.org/10.1007/BF02096933>.
101. N. Read, Short-range Ising spin glasses: The metastate interpretation of replica symmetry breaking, *Phys. Rev. E.* **90**, 032142 (Sep, 2014). doi: 10.1103/PhysRevE.90.032142. URL <https://link.aps.org/doi/10.1103/PhysRevE.90.032142>.
102. K. Hukushima and K. Nemoto, Exchange Monte Carlo method and application to spin glass simulations, *J. Phys. Soc. Japan.* **65**, 1604 (1996). doi: 10.1143/JPSJ.65.1604.
103. E. Marinari. Optimized Monte Carlo methods. In eds. J. Kerstész and I. Kondor, *Advances in Computer Simulation*. Springer-Verlag (1998). doi: 10.1007/BFb0105459.
104. E. Marinari, G. Parisi, and J. J. Ruiz-Lorenzo. Numerical simulations of spin glass systems. In ed. A. P. Young, *Spin Glasses and Random Fields*. World Scientific, Singapore (1998).
105. W. Janke. Monte Carlo simulations in statistical physics – from basic prin-

- ciples to advanced applications. In ed. Yu. Holovatch, Order, Disorder and Criticality, vol. 3, pp. 93-166. World Scientific, Singapore (2013).
106. J. Machta, Population annealing with weighted averages: A Monte Carlo method for rough free-energy landscapes, *Phys. Rev. E* **82**, 026704 (Aug, 2010). doi: 10.1103/PhysRevE.82.026704. URL <https://link.aps.org/doi/10.1103/PhysRevE.82.026704>.
 107. W. Wang, J. Machta, and H. G. Katzgraber, Comparing Monte Carlo methods for finding ground states of Ising spin glasses: Population annealing, simulated annealing, and parallel tempering, *Phys. Rev. E* **92**, 013303 (Jul, 2015). doi: 10.1103/PhysRevE.92.013303. URL <https://link.aps.org/doi/10.1103/PhysRevE.92.013303>.
 108. W. Wang, J. Machta, and H. G. Katzgraber, Population annealing: Theory and application in spin glasses, *Phys. Rev. E* **92**, 063307 (Dec, 2015). doi: 10.1103/PhysRevE.92.063307. URL <https://link.aps.org/doi/10.1103/PhysRevE.92.063307>.
 109. M. Baity-Jesi, R. A. Baños, A. Cruz, L. A. Fernandez, J. M. Gil-Narvion, A. Gordillo-Guerrero, D. Iniguez, A. Maiorano, F. Mantovani, E. Marinari, V. Martín-Mayor, J. Monforte-Garcia, A. Muñoz Sudupe, D. Navarro, G. Parisi, S. Perez-Gaviro, M. Pivanti, F. Ricci-Tersenghi, J. J. Ruiz-Lorenzo, S. F. Schifano, B. Seoane, A. Tarancon, R. Tripicciono, and D. Yllanes, Critical parameters of the three-dimensional Ising spin glass, *Phys. Rev. B* **88**, 224416 (2013). doi: 10.1103/PhysRevB.88.224416.
 110. F. Cooper, B. Freedman, and D. Preston, Solving $\phi_{1,2}^4$ field theory with Monte Carlo, *Nucl. Phys. B* **210**, 210 (1982). doi: 10.1016/0550-3213(82)90240-1.
 111. M. Palassini and S. Caracciolo, Universal finite-size scaling functions in the 3D Ising spin glass, *Phys. Rev. Lett.* **82**, 5128–5131 (1999). doi: 10.1103/PhysRevLett.82.5128.
 112. T. Jörg and H. G. Katzgraber, Evidence for universal scaling in the spin-glass phase, *Phys. Rev. Lett.* **101**, 197205 (2008). doi: 10.1103/PhysRevLett.101.197205.
 113. T. Jörg, H. G. Katzgraber, and F. Krzakala, Behavior of Ising spin glasses in a magnetic field, *Phys. Rev. Lett.* **100**, 197202 (2008). doi: 10.1103/PhysRevLett.100.197202.
 114. T. Jörg and H. G. Katzgraber, Universality and universal finite-size scaling functions in four-dimensional Ising spin glasses, *Phys. Rev. B* **77**, 214426 (2008). doi: 10.1103/PhysRevB.77.214426.
 115. L. Bernardi and I. A. Campbell, Violation of universality for Ising spin-glass transitions, *Phys. Rev. B* **52**, 12501–12504 (Nov, 1995). doi: 10.1103/PhysRevB.52.12501. URL <http://link.aps.org/doi/10.1103/PhysRevB.52.12501>.
 116. E. Marinari, G. Parisi, J. Ruiz-Lorenzo, and F. Ritort, Numerical evidence for spontaneously broken replica symmetry in 3d spin glasses, *Phys. Rev. Lett.* **76**, 843–846 (Jan, 1996). doi: 10.1103/PhysRevLett.76.843. URL <http://link.aps.org/doi/10.1103/PhysRevLett.76.843>.
 117. E. Marinari, G. Parisi, and J. J. Ruiz-Lorenzo, On the phase structure of

- the 3d Edwards-Anderson spin glass, *Phys. Rev. B* **58**, 14852 (1998). doi: 10.1103/PhysRevB.58.14852.
118. R. Alvarez Baños, A. Cruz, L. A. Fernandez, J. M. Gil-Narvion, A. Gordillo-Guerrero, M. Guidetti, A. Maiorano, F. Mantovani, E. Marinari, V. Martín-Mayor, J. Monforte-Garcia, A. Muñoz Sudupe, D. Navarro, G. Parisi, S. Perez-Gaviro, J. J. Ruiz-Lorenzo, S. F. Schifano, B. Seoane, A. Tarancon, R. Tripiccion, and D. Yllanes, Static versus dynamic heterogeneities in the $D = 3$ Edwards-Anderson-Ising spin glass, *Phys. Rev. Lett.* **105**, 177202 (2010). doi: 10.1103/PhysRevLett.105.177202.
 119. P. Contucci, C. Giardinà, C. Giberti, G. Parisi, and C. Vernia, Structure of correlations in three dimensional spin glasses, *Phys. Rev. Lett.* **103**, 017201 (2009). doi: 10.1103/PhysRevLett.103.017201.
 120. S. Caracciolo, G. Parisi, S. Patarnello, and N. Surlas, Low temperature behaviour of 3-d spin glasses in a magnetic field, *J. Phys. France* **51**(17), 1877–1895 (1990). doi: 10.1051/jphys:0199000510170187700. URL <https://doi.org/10.1051/jphys:0199000510170187700>.
 121. D. A. Huse and D. S. Fisher, On the behavior of Ising spin glasses in a uniform magnetic field, *J. Phys. I France* **1**(5), 621–625 (1991). doi: 10.1051/jp1:1991157. URL <https://doi.org/10.1051/jp1:1991157>.
 122. S. Caracciolo, G. Parisi, S. Patarnello, and N. Surlas, On computer simulations for spin glasses to test mean-field predictions, *J. Phys. I France* **1**(5), 627–628 (1991). doi: 10.1051/jp1:1991158. URL <https://doi.org/10.1051/jp1:1991158>.
 123. J.C. Ciria, G. Parisi, F. Ritort, and J.J. Ruiz-Lorenzo, The de Almeida-Thouless line in the four dimensional Ising spin glass, *J. Phys. I France* **3**(11), 2207–2227 (1993). doi: 10.1051/jp1:1993241. URL <https://doi.org/10.1051/jp1:1993241>.
 124. G. Parisi, F. Ricci-Tersenghi, and J. J. Ruiz-Lorenzo, Dynamics of the four-dimensional spin glass in a magnetic field, *Phys. Rev. B* **57**, 13617 (1998). doi: 10.1103/PhysRevB.57.13617.
 125. E. Marinari, G. Parisi, and F. Zuliani, Four-dimensional spin glasses in a magnetic field have a mean-field-like phase, *J. Phys. A: Math. and Gen.* **31**, 1181 (1998). doi: doi:10.1088/0305-4470/31/4/008.
 126. E. Marinari, C. Naitza, and G. Parisi, Critical behavior of the 4d spin glass in magnetic field, *Journal of Physics A: Mathematical and General* **31**, 6355 (1998). doi: 10.1088/0305-4470/31/30/005.
 127. E. Marinari, C. Naitza, F. Zuliani, G. Parisi, M. Picco, and F. Ritort, General method to determine replica symmetry breaking transitions, *Phys. Rev. Lett.* **81**, 1698–1701 (Aug, 1998). doi: 10.1103/PhysRevLett.81.1698. URL <https://link.aps.org/doi/10.1103/PhysRevLett.81.1698>.
 128. J. Houdayer and O. C. Martin, Ising spin glasses in a magnetic field, *Phys. Rev. Lett.* **82**, 4934–4937 (Jun, 1999). doi: 10.1103/PhysRevLett.82.4934. URL <https://link.aps.org/doi/10.1103/PhysRevLett.82.4934>.
 129. E. Marinari, G. Parisi, and F. Zuliani, Comment on “Ising spin glasses in a magnetic field”, *Phys. Rev. Lett.* **84**, 1056–1056 (Jan, 2000). doi: 10.1103/PhysRevLett.84.1056. URL <https://link.aps.org/doi/10.1103/>

- PhysRevLett.**84**.1056.
130. J. Houdayer and O. C. Martin, Houdayer and Martin reply:, *Phys. Rev. Lett.* **84**, 1057–1057 (Jan, 2000). doi: 10.1103/PhysRevLett.84.1057. URL <https://link.aps.org/doi/10.1103/PhysRevLett.84.1057>.
 131. A. Cruz, L. A. Fernández, S. Jiménez, J. J. Ruiz-Lorenzo, and A. Tarancón, Off-equilibrium fluctuation-dissipation relations in the 3d Ising spin glass in a magnetic field, *Phys. Rev. B.* **67**, 214425 (Jun, 2003). doi: 10.1103/PhysRevB.67.214425. URL <http://link.aps.org/doi/10.1103/PhysRevB.67.214425>.
 132. A. P. Young and H. G. Katzgraber, Absence of an Almeida-Thouless line in three-dimensional spin glasses, *Phys. Rev. Lett.* **93**, 207203 (2004). doi: 10.1103/PhysRevLett.93.207203.
 133. L. Leuzzi, G. Parisi, F. Ricci-Tersenghi, and J. J. Ruiz-Lorenzo, Dilute one-dimensional spin glasses with power law decaying interactions, *Phys. Rev. Lett.* **101**, 107203 (Sep, 2008). doi: 10.1103/PhysRevLett.101.107203. URL <http://link.aps.org/doi/10.1103/PhysRevLett.101.107203>.
 134. R. A. Baños, A. Cruz, L. A. Fernandez, J. M. Gil-Narvion, A. Gordillo-Guerrero, M. Guidetti, D. Iniguez, A. Maiorano, E. Marinari, V. Martín-Mayor, J. Monforte-Garcia, A. Muñoz Sudupe, D. Navarro, G. Parisi, S. Perez-Gaviro, J. J. Ruiz-Lorenzo, S. F. Schifano, B. Seoane, A. Tarancon, P. Tellez, R. Tripiccion, and D. Yllanes, Thermodynamic glass transition in a spin glass without time-reversal symmetry, *Proc. Natl. Acad. Sci. USA.* **109**, 6452 (2012). doi: 10.1073/pnas.1203295109.
 135. M. Baity-Jesi, R. A. Baños, A. Cruz, L. A. Fernandez, J. M. Gil-Narvion, A. Gordillo-Guerrero, D. Iniguez, A. Maiorano, M. F., E. Marinari, V. Martín-Mayor, J. Monforte-Garcia, A. Muñoz Sudupe, D. Navarro, G. Parisi, S. Perez-Gaviro, M. Pivanti, F. Ricci-Tersenghi, J. J. Ruiz-Lorenzo, S. F. Schifano, B. Seoane, A. Tarancon, R. Tripiccion, and D. Yllanes, Dynamical transition in the d=3 Edwards-Anderson spin glass in an external magnetic field, *Phys. Rev. E.* **89**, 032140 (2014). doi: 10.1103/PhysRevE.89.032140.
 136. M. Baity-Jesi, R. A. Baños, A. Cruz, L. A. Fernandez, J. M. Gil-Narvion, A. Gordillo-Guerrero, D. Iniguez, A. Maiorano, M. F., E. Marinari, V. Martín-Mayor, J. Monforte-Garcia, A. Muñoz Sudupe, D. Navarro, G. Parisi, S. Perez-Gaviro, M. Pivanti, F. Ricci-Tersenghi, J. J. Ruiz-Lorenzo, S. F. Schifano, B. Seoane, A. Tarancon, R. Tripiccion, and D. Yllanes, The three dimensional Ising spin glass in an external magnetic field: the role of the silent majority, *J. Stat. Mech.* **2014**, P05014 (2014). doi: 10.1088/1742-5468/2014/05/P05014.
 137. M. Mézard and G. Parisi, The Bethe lattice spin glass revisited, *Eur. Phys. J. B.* **20**, 217 (2001). doi: 10.1007/PL00011099.
 138. H. Takahashi, F. Ricci-Tersenghi, and Y. Kabashima, Finite-size scaling of the de Almeida–Thouless instability in random sparse networks, *Physical Review B.* **81**(17), 174407 (2010).
 139. G. Parisi and F. Ricci-Tersenghi, A numerical study of the overlap probability distribution and its sample-to-sample fluctuations in a mean-field model,

- Philosophical Magazine.* **92**(1-3), 341–352 (2012).
140. F. Belletti, M. Cotallo, A. Cruz, L. A. Fernandez, A. Gordillo-Guerrero, M. Guidetti, A. Maiorano, F. Mantovani, E. Marinari, V. Martín-Mayor, A. M. Sudupe, D. Navarro, G. Parisi, S. Perez-Gaviro, J. J. Ruiz-Lorenzo, S. F. Schifano, D. Sciretti, A. Tarancon, R. Tripicciono, J. L. Velasco, and D. Yllanes, Nonequilibrium spin-glass dynamics from picoseconds to one tenth of a second, *Phys. Rev. Lett.* **101**, 157201 (2008). doi: 10.1103/PhysRevLett.101.157201.
 141. A. Cruz, L. A. Fernandez, A. Gordillo-Guerrero, M. Guidetti, A. Maiorano, F. Mantovani, E. Marinari, V. Martín-Mayor, A. Muñoz Sudupe, D. Navarro, G. Parisi, S. Perez-Gaviro, J. J. Ruiz-Lorenzo, S. F. Schifano, D. Sciretti, A. Tarancon, R. Tripicciono, D. Yllanes, and A. P. Young, The spin glass phase in the four-state, three-dimensional Potts model, *Phys. Rev. B.* **79**, 184408 (2009). doi: 10.1103/PhysRevB.79.184408.
 142. R. A. Baños, A. Cruz, L. A. Fernandez, J. M. Gil-Narvion, A. Gordillo-Guerrero, M. Guidetti, D. Iñiguez, A. Maiorano, F. Mantovani, E. Marinari, V. Martín-Mayor, J. Monforte-Garcia, A. Muñoz Sudupe, D. Navarro, G. Parisi, S. Perez-Gaviro, F. Ricci-Tersenghi, J. J. Ruiz-Lorenzo, S. F. Schifano, B. Seoane, A. Tarancón, R. Tripicciono, and D. Yllanes, Sample-to-sample fluctuations of the overlap distributions in the three-dimensional Edwards-Anderson spin glass, *Phys. Rev. B.* **84**, 174209 (Nov, 2011). doi: 10.1103/PhysRevB.84.174209. URL <http://link.aps.org/doi/10.1103/PhysRevB.84.174209>.
 143. M. Baity-Jesi, E. Calore, A. Cruz, L. A. Fernandez, J. M. Gil-Narvión, A. Gordillo-Guerrero, D. Iiguez, A. Maiorano, E. Marinari, V. Martin-Mayor, J. Monforte-Garcia, A. Muoz Sudupe, D. Navarro, G. Parisi, S. Perez-Gaviro, F. Ricci-Tersenghi, J. J. Ruiz-Lorenzo, S. F. Schifano, B. Seoane, A. Tarancón, R. Tripicciono, and D. Yllanes, A statics-dynamics equivalence through the fluctuationdissipation ratio provides a window into the spin-glass phase from nonequilibrium measurements, *Proceedings of the National Academy of Sciences.* **114**(8), 1838–1843 (2017). doi: 10.1073/pnas.1621242114. URL <http://www.pnas.org/content/114/8/1838.abstract>.
 144. M. Baity-Jesi, E. Calore, A. Cruz, L. A. Fernandez, J. M. Gil-Narvión, A. Gordillo-Guerrero, D. Iñiguez, A. Lasanta, A. Maiorano, E. Marinari, V. Martin-Mayor, J. Moreno-Gordo, A. Muñoz Sudupe, D. Navarro, G. Parisi, S. Perez-Gaviro, F. Ricci-Tersenghi, J. J. Ruiz-Lorenzo, S. F. Schifano, B. Seoane, A. Tarancón, R. Tripicciono, and D. Yllanes, The Mpemba effect in spin glasses is a persistent memory effect, *Proceedings of the National Academy of Sciences.* **116**(31), 15350–15355 (2019). ISSN 0027-8424. doi: 10.1073/pnas.1819803116. URL <https://www.pnas.org/content/116/31/15350>.
 145. F. Belletti, F. Mantovani, G. Poli, S. F. Schifano, R. Tripicciono, I. Campos, A. Cruz, D. Navarro, S. Perez-Gaviro, D. Sciretti, A. Tarancon, J. L. Velasco, P. Tellez, L. A. Fernandez, V. Martín-Mayor, A. Muñoz Sudupe, S. Jimenez, A. Maiorano, E. Marinari, and J. J. Ruiz-Lorenzo, Ianus:

- And adaptive fpga computer, *Computing in Science and Engineering*. **8**, 41 (2006).
146. F. Belletti, M. Cotallo, A. Cruz, L. A. Fernandez, A. Gordillo, A. Maiorano, F. Mantovani, E. Marinari, V. Martín-Mayor, A. Muñoz Sudupe, D. Navarro, S. Perez-Gaviro, J. J. Ruiz-Lorenzo, S. F. Schifano, D. Sciretti, A. Tarancon, R. Tripiccione, and J. L. Velasco, Simulating spin systems on IANUS, an FPGA-based computer, *Comp. Phys. Comm.* **178**, 208–216 (2008). doi: 10.1016/j.cpc.2007.09.006.
 147. F. Belletti, M. Guidetti, A. Maiorano, F. Mantovani, S. F. Schifano, R. Tripiccione, M. Cotallo, S. Perez-Gaviro, D. Sciretti, J. L. Velasco, A. Cruz, D. Navarro, A. Tarancon, L. A. Fernandez, V. Martín-Mayor, A. Muñoz-Sudupe, D. Yllanes, A. Gordillo-Guerrero, J. J. Ruiz-Lorenzo, E. Marinari, G. Parisi, M. Rossi, and G. Zanier, Janus: An FPGA-based system for high-performance scientific computing, *Computing in Science and Engineering*. **11**, 48 (2009). doi: 10.1109/MCSE.2009.11.
 148. M. Baity-Jesi, R. A. Baños, A. Cruz, L. A. Fernandez, J. M. Gil-Narvion, A. Gordillo-Guerrero, M. Guidetti, D. Iniguez, A. Maiorano, F. Mantovani, E. Marinari, V. Martín-Mayor, J. Monforte-Garcia, A. Muñoz Sudupe, D. Navarro, G. Parisi, M. Pivanti, S. Perez-Gaviro, F. Ricci-Tersenghi, J. J. Ruiz-Lorenzo, S. F. Schifano, B. Seoane, A. Tarancon, P. Tellez, R. Tripiccione, and D. Yllanes, Reconfigurable computing for Monte Carlo simulations: Results and prospects of the Janus project, *Eur. Phys. J. Special Topics*. **210**, 33 (AUG, 2012). doi: 10.1140/epjst/e2012-01636-9.
 149. M. Baity-Jesi, R. A. Baños, A. Cruz, L. A. Fernandez, J. M. Gil-Narvion, A. Gordillo-Guerrero, D. Iniguez, A. Maiorano, F. Mantovani, E. Marinari, V. Martín-Mayor, J. Monforte-Garcia, A. Muñoz Sudupe, D. Navarro, G. Parisi, S. Perez-Gaviro, M. Pivanti, F. Ricci-Tersenghi, J. J. Ruiz-Lorenzo, S. F. Schifano, B. Seoane, A. Tarancon, R. Tripiccione, and D. Yllanes, Janus II: a new generation application-driven computer for spin-system simulations, *Comp. Phys. Comm.* **185**, 550–559 (2014). doi: 10.1016/j.cpc.2013.10.019.